Structure of the Santo Domingo Basin and La Bajada Constriction Area, New Mexico

By Scott A. Minor, Mark R. Hudson, V.J.S. Grauch, and David A. Sawyer

Chapter E of
The Cerrillos Uplift, the La Bajada Constriction, and Hydrogeologic Framework of the Santo Domingo Basin, Rio Grande Rift, New Mexico
Edited by Scott A. Minor

Professional Paper 1720–E

U.S. Department of the Interior
U.S. Geological Survey

Contents

Figures

Table

Structure of the Santo Domingo Basin and La Bajada Constriction Area, New Mexico

By Scott A. Minor, Mark R. Hudson, V.J.S. Grauch, and David A. Sawyer

Abstract

The Santo Domingo Basin, located within the Rio Grande rift in northern New Mexico, is topographically subdued and structurally distinct compared with the adjacent Española and northern Albuquerque rift basins, yet it contains structural elements in common with both neighboring basins. A northeast elongation of the Santo Domingo Basin is expressed along its northwestern and southeastern margins by partly buried, relatively large displacement, northeast-striking faults and fault segments that merge with large north-striking fault zones bordering the adjacent basins. Internally, the Santo Domingo Basin exhibits a symmetric, semiconcentric, inward-dipping fault pattern that is centered on the deepest part of the basin as defined by a gravity low. Geologic age relations on the margins of the Española, Santo Domingo, and northern Albuquerque Basins suggest that active border faulting progressively migrated basinward during the Neogene. This relation is clearly demonstrated on the east shoulder of the Santo Domingo Basin by the Tetilla fault zone, an early rift-border and extensional-transfer structure that was abandoned sometime before about 2.5 Ma as basin-margin subsidence was taken up on the La Bajada fault zone farther west. Owing to basinward migration of faulting in the Santo Domingo Basin, intrabasin faults may have longer growth-fault histories and larger dip-slip displacements in the subsurface compared with the border faults, an interpretation supported by the presence of pronounced gravity gradients well basinward of the outer border faults. Fault slickenline observations indicate that most basinal faults formed with nearly pure normal slip and that many of these faults were reactivated with greater components of strike-slip motion. Oblique- and strike-slip reactivated normal faults, concentrated near the northwestern and southeastern basin margins, may be related to the lateral transfer of extensional strain to adjoining basins. Paleomagnetic results from the Tetilla fault zone suggest that such strain transfer is at least locally accommodated by inclined-axis rotation of fault blocks.

In the northeastern part of the Santo Domingo Basin in the area of the La Bajada constriction, northwest-striking overlapping faults of opposing dip project into the basin from opposite sides but die out along strike. These faults include young scalloped splays of the northern La Bajada fault zone and the opposite-dipping, newly defined Sanchez fault. Although these faults do not provide complete structural closure of the northeast end of the basin, they may locally redirect and retard southerly, down-gradient flow of ground water through the constriction area. A series of segmented, right-stepping, faulted antiforms and grabens within the La Bajada constriction track the northeastward migration of the local rift axis.

Fault zones in the Santo Domingo Basin area are characterized by outer damage zones, which typically contain strike-parallel minor fractures that may either enhance or impede groundwater flow along the faults, and by centrally located, low permeability, clay-rich fault cores that likely impede cross-fault flow. Host-rock lithologies strongly influence the width of fault-zone components and control variations in fracturing and other brittle-strain features. An abundance of asymmetrically distributed fault-zone cements indicates that fault-parallel and fault-compartmentalized groundwater flow was, and may continue to be, common in the basin aquifers. The Santo Domingo Basin contains many faults of varied geometry, internal structure, and cement distribution that impart significant heterogeneity of permeability within the basin aquifer.

Introduction

Studies by the U.S. Geological Survey were begun in 1996 to improve understanding of the geologic framework of the Albuquerque composite basin and adjoining areas, in order that more accurate hydrogeologic parameters could be applied to new hydrologic models. The ultimate goal of this multidisciplinary effort has been to provide better quantify estimates of future water supplies for northern New Mexico's growing urban centers, which largely subsist on aquifers in the Rio Grande rift basin (Bartolino and Cole, 2002). From preexisting hydrologic models it became evident that hydrogeologic uncertainties were large in the Santo Domingo Basin area, immediately upgradient from the greater Albuquerque metropolitan area, and particularly in the northeast part of the basin referred to as the La Bajada constriction (see chapter A, this volume, for a geologic definition of this feature as used in this report). Accordingly, a priority for new geologic and geophysical investigations was to better determine the hydrogeologic framework of the La Bajada constriction area. This chapter, along with the other chapters of this report, presents the results of such investigations as recently conducted by the U.S. Geological Survey.

In this chapter we describe and interpret the salient structural features of the Santo Domingo rift basin and overlapping La Bajada constriction and the geometry and kinematics of intrabasin faults. (The reader is referred to chapter A of this report for preliminary geographic and geologic definitions and descriptions of the Santo Domingo Basin, La Bajada constriction, intrabasin structural blocks, and rift-flank uplifted blocks.) An understanding of the structural configuration and structure-induced anisotropy and heterogeneity of the basin and constriction helps elucidate the geologic controls on ground-water flow within and between basins. Below we describe and interpret the fault architecture of the overall Santo Domingo Basin to provide geologic and tectonic context for more detailed discussions that follow of the La Bajada constriction and adjacent uplifted structural blocks. Spatial-temporal patterns of faulting throughout the basin are also discussed. The structural geometry of the La Bajada constriction area is addressed in detail, including the configuration and significance of major, partly concealed, bordering fault zones. Finally, the structural characteristics and cement patterns of fault zones surveyed within the Santo Domingo Basin are summarized, and we then assess the influence that they may have on ancient and modern ground-water flow.

Santo Domingo Basin Structural Framework

Regional Tectonic Setting

The late Cenozoic Rio Grande rift (fig. A1) is an extensional tectonic feature of the Basin and Range structural province (Wernicke, 1992). Temporal changes in the geometry and kinematics of rift faults are commonly related to Neogene clockwise rotation of the regional direction of tectonic extension or the horizontal least principal stress axis (Aldrich, Chapin, and Laughlin, 1986; Chapin and Cather, 1994), which is widely recognized throughout the Basin and Range province (Zoback, Anderson, and Thompson, 1981). Some workers have linked the tectonic history of the rift to northward translation and clockwise rotation of the Colorado Plateau (Hamilton and Myers, 1966; Cather, 1997; Wawrzyniec and others, 2002) (fig. A1). In this interpretation, the rift is a localized transtensional tectonic feature that has accommodated both extension and dextral transcurrent movement along the eastern margin of the plateau block (Wawrzyniec and others, 2002).

The middle part of the Rio Grande rift that is the focus of the present study consists of three structurally linked, north-trending, right-stepping, en echelon extensional basins that formed mainly during the Neogene (Kelley, 1982; Chapin and Cather, 1994). From south to north, they are the northern Albuquerque Basin, Santo Domingo Basin; and Española Basin (figs. A1, A2). Growth faults are common in these basins, implying that faulting and sedimentation were broadly coeval during basin formation (May and Russell, 1994; Connell, Koning, and Cather, 1999). Most basins of the Rio Grande rift in northern New Mexico and southern Colorado form an en echelon chain of half grabens that alternately face east and west (Chapin and Cather, 1994; Russell and Snelson, 1994). The northern Albuquerque Basin is a poorly defined half graben in which basin-fill sediments are mostly tilted gently to the east and are cut on the east side by west-dipping normal faults, including the large-displacement Rincon fault (RC) whose footwall block is expressed by the precipitous front of the Sandia Mountains (Kelley, 1977) (figs. A2, E1). The half-graben structural geometry of the Española Basin is better developed than that of the northern Albuquerque Basin and the graben is tilted in the opposite direction (west) (Kelley, 1982; Chapin and Cather, 1994). The large down-to-east Pajarito fault (PJ) forms the recent western boundary of the Española Basin and marks the eastern limit of the Jemez Mountains within its footwall block (fig. A2).

Structural Geometry

The topographically subdued Santo Domingo Basin is structurally distinct from the adjoining Española and northern Albuquerque Basins, and yet it contains structural elements that appear to be inherited from both. North of the Santa Ana Mesa volcanic field (SAMVF, fig. A2) the Santo Domingo Basin possesses an antiformal fault-block geometry, in which down-to-west normal faults and gentle (<15°) eastward stratal dips prevail in the eastern part of the basin and opposing fault displacements and stratal dips dominate in the northwestern part (figs. A2, E1) (Smith, McIntosh, and Kuhle, 2001). The same pattern of opposing (that is, down-to-basin) fault displacements continue into the southern part of the basin (fig. E1), but strata in this part of the basin form a gently eastward-dipping homocline tilted towards the basin-bounding San Francisco fault (SF, fig. E1) regardless of the dip directions of local intrabasinal faults (Kelly, 1977). The eastward dips of strata in the southernmost part of the basin are similar to dips of strata

Figure E1 (facing page). Northern Albuquerque and Santo Domingo Basins showing major intrabasin and basin-bounding faults. Faults based on an unpublished regional fault compilation by M.R Hudson, S.A. Minor, and V.J.S. Grauch; see Hudson and others (1999) for sources of data. Basin boundaries are based largely on isostatic residual gravity data of Grauch, Gillespie, and Keller (1999). Geophysical data used to infer concealed faults are discussed in text and in chapters D and F, this volume. Faults and fault zones: AD, Algodones; BR, Borrego; CA, Camada; CC, Cañada de Cochiti; CO, Cochiti; EC, Escala; EH, East Heights; EZ, East Ziana; HE, Hagan Embayment; JZ, Jemez; LB, La Bajada; PB, Pico Butte; PJ, Pajarito; PL, Placitas; RC, Rincon; SA, Santa Ana; SC, Sanchez; SH, Sand Hill; SI, Sile; SF, San Francisco; SL, South Luce; SP, South Pajarito; SY, San Ysidro; TJ, Tijeras; TM, Tamaya; TT, Tetilla; VV, Valley View; WZ, West Ziana; ZC, Zia County Dump.

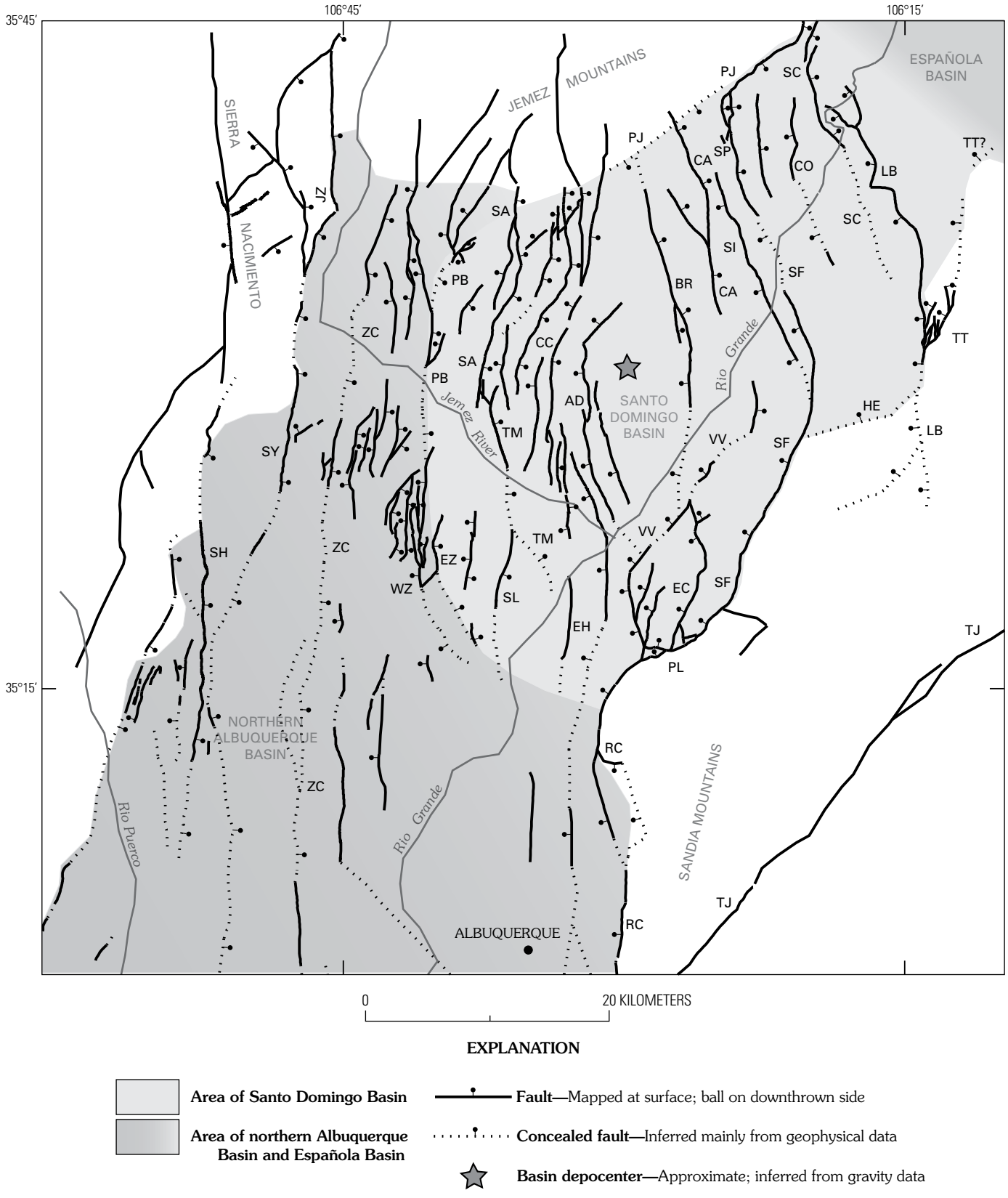
35°45′
106°45′
106°15′
35°15′
SIERRA NACIMIENTO
JEMEZ MOUNTAINS
ESPAÑOLA BASIN
SANTO DOMINGO BASIN
NORTHERN ALBUQUERQUE BASIN
SANDIA MOUNTAINS
ALBUQUERQUE
Rio Grande
Jemez River
Rio Puerco
JZ
SY
SH
ZC
PB
SA
CC
AD
TM
EZ
WZ
SL
EH
PJ
SC
SP
CA
CO
LB
TT?
TT
SI
BR
SF
VV
HE
EC
PL
RC
TJ
0
20 KILOMETERS
EXPLANATION
Area of Santo Domingo Basin
Area of northern Albuquerque Basin and Española Basin
Fault—Mapped at surface; ball on downthrown side
Concealed fault—Inferred mainly from geophysical data
Basin depocenter—Approximate; inferred from gravity data

in adjoining parts of the northern Albuquerque Basin. Down-to-west faults are more common and have longer traces and greater throws near the southeast and east borders of the Santo Domingo Basin, compared with down-to-east faults, which are more abundant and have longer traces and greater throws near the northwest and west basin borders (fig. E1). Toward the basin center the dominance of one direction of fault dip is diminished and replaced by overlapping or interleaved faults that may dip in either direction (Smith, McIntosh, Kuhle, 2001). The San Francisco (SF) fault bounding the southeast side of the basin connects by means of the Placitas fault (PL) into the Rincon fault (RC), which is the master fault that bounds the Albuquerque Basin half graben (fig. A2, E1). In similar fashion, the Pajarito fault (PJ) bordering the northwest side of the Santo Domingo Basin becomes the master bounding fault of the Española half-graben basin to the north. Thus, fundamental bounding structures of all three basins are structurally linked.

The regional fault compilation shown in figure E1, partly based on high-resolution aeromagnetic data (fig. D5) (Grauch, 1999; chapter D, this volume), reveals within the Santo Domingo Basin a symmetric, semiconcentric fault pattern that is centered on the east-central part of the late Pliocene Santa Ana Mesa volcanic field (SAMVF, fig. A2). The center of this semicircular fault pattern also coincides with the deepest part of the basin, or depocenter (star symbol, fig. E1), defined by isostatic residual gravity (pl. 3, fig. A3) (Grauch, Gillespie, and Keller, 1999). Furthermore, some of the larger semicircular down-to-east faults (Pico Butte (PB)–East Ziana (EZ), Santa Ana (SA)–Tamaya (TM), and Cañada de Cochiti (CC) faults) and down-to-west faults (San Francisco (SF), Sile (SI) and La Bajada (LB) faults) form a crude, opposing, inward-hooking pattern in map view (figs. A2, A3, E1).

Regional gravity data and topography indicate that the Santo Domingo Basin is elongate in a northeast-southwest direction despite the northerly strike of many intrabasin faults (figs. A2, A3, E1) (see also gravity discussion in chapter D, this volume). The southeast and northwest margins of the Santo Domingo Basin are marked by moderate- to large-displacement faults that curve, bend, or splay into northeasterly strikes, parallel to the direction of basin elongation, and collectively define the structural borders of those sides of the basin. Examples include the Placitas (PL), southern San Francisco (SF), Valley View (VV), and Hagan Bench (HB) faults (southeast margin) and the northern Pico Butte (PB), Santa Ana (SA), southern Cañada de Cochiti (CC), and Pajarito (PJ) faults (northwest margin) (figs. A2, A3, E1). A concealed southwest extension of the Pajarito fault inferred from a coincident strong linear gravity gradient (fig. A3) (see chapter D, this volume) forms part of the northwest border of the Santo Domingo basin and may structurally link with a northeast-striking segment of the Santa Ana fault (figs. A2, E1). Thus, the northeast-elongated nature of the basin appears to be structurally expressed along its northwest and southeast margins by partly buried, relatively large displacement, northeast-striking faults and fault segments. Crosscutting and overlapping relations of faults and young basin-fill sediments and volcanic rocks, particularly on the northwest side of the basin, indicate that movement along many of the semicircular, northerly striking faults within the Santo Domingo Basin continued after movement ceased on northeast-striking basin-margin faults.

In contrast to its northeast-trending elongated sides, the Santo Domingo Basin is not completely bounded by faults along its narrower southern and northeast margins. The southwest part of the Santo Domingo Basin is separated from the northern Albuquerque Basin by the Ziana horst (Ziana anticline of Kelly, 1977), a relatively uplifted, fault-bounded, north-trending structural culmination or ridge that has negligible topographic expression (fig. A2) but forms a moderate linear gravity high (fig. A3). The Ziana structural ridge can be projected continuously northward on the basis of gravity data into the footwall block of the basin-bordering Pico Butte (PB) fault (figs. A2, A3). To the south the West Ziana (WZ) and East Ziana (EZ) faults, which bound the Ziana horst, and the nearby Tamaya (TM) fault curve in a concentric manner and project southeastward as inferred from subtle linear aeromagnetic anomalies nearly to the Rio Grande (pl. 4, fig. A2), but the faults do not appear to extend all the way to the southeastern basin-bounding Rincon fault (RC). Thus, the southern end of the Santo Domingo Basin does not appear to be entirely fault bounded even though a broad, weak gravity high separates this part of the basin from the northern Albuquerque Basin (fig. D1; chapter D, this volume). In the northeast Santo Domingo Basin the northwest-striking Sile (SI) and northern San Francisco (SF) faults (figs. A2, A3, E1) separate a deep, main part of the basin from the shallower Hagan bench (fig. D4). The Sile and San Francisco faults do not project across the entire width of the basin, and northeast of them, within the area of the La Bajada constriction, northwest-striking and complexly interleaved faults with opposing dips similarly extend only part way across the basin (fig. E1). Therefore, the aggregate fault network in the constriction area, which is discussed in more detail below, does not form a complete structural barrier between the Santo Domingo Basin and adjacent Española Basin.

Strike and dip were measured on principal slip planes in the cores of numerous fault zones exposed in the Santo Domingo and northern Albuquerque Basins to further characterize the geometry and configuration of intrabasin faults and, along with slip measurements, to investigate fault kinematics (see following section). Most fault planes dip between 55° and 77° (66° mean) (fig. E2). Within the Santo Domingo Basin, faults mostly dip towards the basin center, consistent with the relatively symmetrical fault geometry of the basin. Most fault surfaces are planar at outcrop scale, but several, mainly larger displacement (that is, >100 m), fault surfaces possess large mullions that trend subparallel to the principal slip direction and create curvilinear fault traces.

Dip-slip displacement on individual faults within and bordering the Santo Domingo Basin ranges from less than 10 m to more than 4,000 m at surface exposures, although most faults have dip displacements of less than 100 m. Displacement diminishes along strike towards fault terminations as

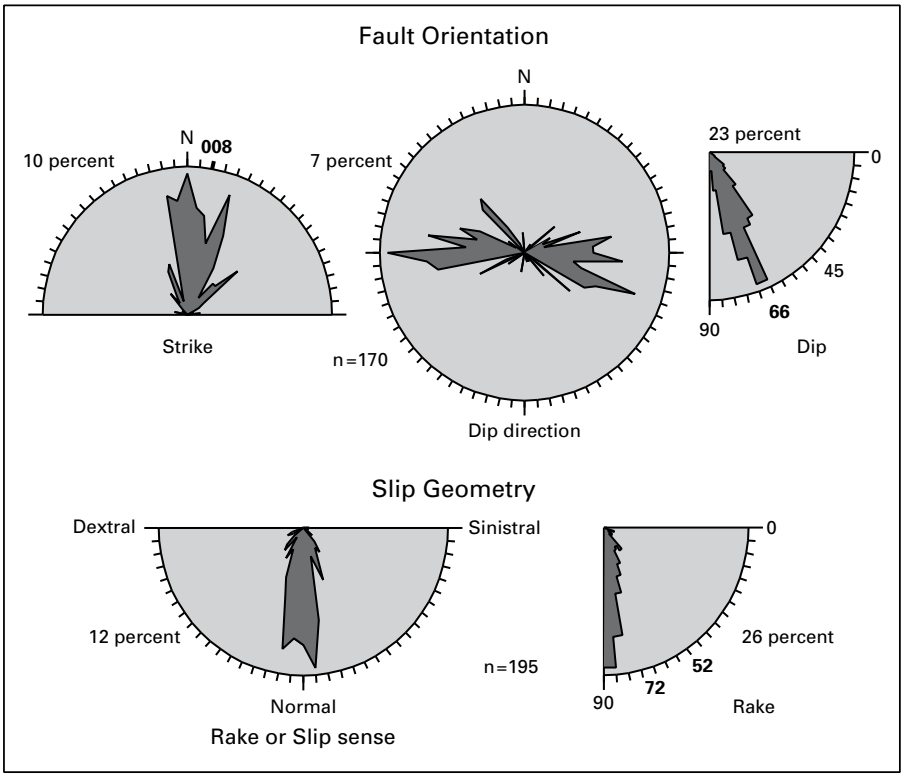

Figure E2. Frequency of orientation and slip geometry of faults in Santo Domingo and northern Albuquerque Basins. Percentage next to each diagram indicates relative maximum radius; numbers in bold indicate mean strike, dip, and rake values. Faults dominantly strike north (008° mean), dip moderately (66° mean) east or west, and have normal slip sense (72° mean rake). Overprinted, generally lower rake slickenlines (52° mean) indicate reactivation of many faults by normal-oblique slip.

increasing amounts of extensional strain are accommodated by adjacent overlapping or en echelon faults of opposing or same dip direction. As a result of growth faulting, the footwall blocks of many, and perhaps most, basin faults have experienced greater cumulative dip displacements than indicated by stratigraphic offsets observed at the surface. Faults with the largest surface displacements (>250 m) and longest traces (>25 km) are concentrated along or near the margins of the basin (figs. A2, E1). Surface traces of several large basin-border faults (La Bajada (LB), Hagan Bench (HB), San Francisco (SF), and East Ziana (EZ)–Pico Butte (PB) faults) are positioned 3–7 km outward of the strong gradients defining the perimeter of the northeast-trending main-basin gravity low (fig. A3). This configuration suggests that the greatest dip slip and basin subsidence occurred along faults such as the Santa Ana (SA), Tamaya (TM), and Valley View (VV) that are concentric with, but located a short distance basinward of, the outer border faults (fig. A3). These inner basin margin faults have smaller surface displacements than the >1.5 km of throw that must be accommodated along them at depth, as is implied by large coincident gravity gradients (chapter D, this volume). Such differential vertical displacement is consistent with growth-fault geometries that have been observed throughout the middle Rio Grande rift (May and Russell, 1994).

Faults and Faulting

Kinematics

Determination of the kinematic history (that is, changes in slip sense and slip geometry) of faults in the Santo Domingo Basin provides clues about the evolving roles of faults within the tectonic framework of the Rio Grande rift. Rake angles of slickenlines (striations) observed on faults in the Santo Domingo Basin have a mean of about 75°, and their mode is 85°–90° (fig. E2) (Minor and Hudson, 2006).

These data, together with the senses of slip revealed by offset stratigraphic units, indicate that most of the faults underwent nearly pure normal slip (fig. E2). Nevertheless, a considerable number of fault surfaces contain younger (crosscutting) normal-oblique slickenlines (rake=30°–60°) or even strike-slip slickenlines (rake ≤30°), indicating that many normal faults were reactivated with greater components of strike-slip motion (Minor and Hudson, 2006). Preliminary analysis of the fault-slip data indicates that the overprinted strike-slip patterns in the Santo Domingo Basin are not mainly the result of an Neogene clockwise rotation of the regional stress field (Zoback, Anderson, and Thompson, 1981), which would have resulted in a basin-wide progressive overprinting of northerly striking sinistral-slip faults and slickenlines by dextral-slip faults and slickenlines. No basin-wide statistical correlation of strike-slip sense with fault strike has been found, although components of dextral slip were observed over a broader range of fault strikes (northwest to northeast) than components of sinistral slip (north to northeast). In local structural domains, either dextral slip components (such as north of Santa Ana Mesa volcanic field) or sinistral slip components (such as southeastern border faults of Santo Domingo Basin) are dominant on faults within a certain strike range. Primary and overprinted oblique-slip and strike-slip slickenlines are concentrated in two fault belts near the northwestern and southeastern margins of the Santo Domingo Basin (fig. E3). The northwestern belt is on trend with a cluster of moderate-rake faults along the western margin of the northern Albuquerque Basin. Oblique slip and strike slip presumably facilitated lateral transfer of extensional strain between structurally linked en echelon basins such as those along the middle Rio Grande rift (Faulds and Varga, 1998; Minor and Sawyer, 1999; Chamberlin, 1999). In the Santo Domingo Basin, the existence of oblique- and strike-slip reactivated normal faults near the northwest and southeast basin margins may also be related to another factor: local rotation of fault blocks or principal stress trajectories (or both). Such rotation may have been produced by concentrated lateral shear owing to large extensional strain gradients along the basin margins. Our Santo Domingo fault-slip observations, in particular the evidence for interspersed dextral and sinistral slip components, do not clearly support regional synrift dextral transtension as proposed by Wawrzyniec and others (2002).

Structure of Tetilla and La Bajada Fault Zones

Excellent exposures in the footwall escarpment of the La Bajada fault zone south of Cañada de Santa Fe (pls. 1, 2; fig. A4) allow detailed structural characterization of the Tetilla fault zone, which may have a structural history and geometry similar to those of other early northeast-striking faults bordering the Santo Domingo and northern Albuquerque rift basins. The Tetilla fault zone is inferred to have formed the eastern border of the Santo Domingo basin in Miocene and Pliocene(?) time before basin-border fault subsidence was transferred to the north-striking La Bajada fault zone (Minor and Sawyer, 1999; Sawyer and others, 2002). The 1.2-km-wide Tetilla fault zone consists of north-northeast- to northeast-striking, mainly down-to-basin faults that cut north- to northwest-dipping Eocene to Miocene sedimentary and volcanic rocks (Galisteo (unit Tg), Espinaso (unit Te), and Abiquiu (unit Tab) Formations) (fig. E4). Faults of the Tetilla zone project northeastward beneath, but do not cut, the younger capping 2.7–2.4-Ma basalt flows of the Cerros del Rio volcanic field. The easternmost down-to-basin fault juxtaposes Eocene to Miocene rocks and synrift basin fill against Mesozoic rocks, and it projects northeastward beneath the basalt flows to a northerly strike in Cañada de Santa Fe (fig. E4). Several smaller north-northeast-striking faults, in turn, branch northward from this eastern border fault (fig. E4). North of Cañada de Santa Fe, the north-striking border fault of the Tetilla fault zone can be projected under Cerros del Rio basalt flows on the basis of surface geologic constraints, aeromagnetic lineaments, and subsurface electromagnetic data indicating abrupt westward thickening of buried Santa Fe Group sediments (pl. 2, fig. D7) (see also cross section C-C′, pl. 6; chapter G, this volume). Electromagnetic data (chapter F, this volume) also suggest that this north-striking boundary fault may extend north of Tetilla Peak under the basalt flows and curve eastward into, and structurally link with, a northeast-striking fault or fault zone that accommodates about 650 m of down-to-north displacement of the basal Santa Fe Group contact with underlying Mancos Shale (pl. 2, fig. F4*A*) (cross sections B-B′ and E-E′, pl. 6). Although this inferred buried fault zone can not be confidently projected farther northeast without additional subsurface data, it plausibly may connect with one or more major structures in the southwestern part of the Española Basin. Thus, the Tetilla fault zone represents an older (earlier than 2.7 Ma) rift-border fault system that may have transferred extensional strain between the Santo Domingo and adjacent Española Basins.

Figure E3 (facing page). Major faults in Santo Domingo Basin region; fault-plane exposures with lower angle slickenline rakes or overprinted slickenlines (or both) are marked. Such faults are concentrated along northwest and southeast margins of Santo Domingo Basin. Faults based on an unpublished regional fault compilation by M.R Hudson, S.A. Minor, and V.J.S. Grauch; see Hudson and others (1999) for sources of data. Basin boundaries are based largely on isostatic residual gravity data of Grauch, Gillespie, and Keller (1999). Geophysical data used to infer concealed faults are discussed in text and in chapters D and F, this volume. Faults and fault zones: AD, Algodones; BR, Borrego; CA, Camada; CC, Cañada de Cochiti; CO, Cochiti; EC, Escala; EH, East Heights; EZ, East Ziana; HE, Hagan Embayment; JZ, Jemez; LB, La Bajada; PB, Pico Butte; PJ, Pajarito; PL, Placitas; RC, Rincon; SA, Santa Ana; SC, Sanchez; SH, Sand Hill; SI, Sile; SF, San Francisco; SL, South Luce; SP, South Pajarito; SY, San Ysidro; TJ, Tijeras; TM, Tamaya; TT, Tetilla; VV, Valley View; WZ, West Ziana; ZC, Zia County Dump.

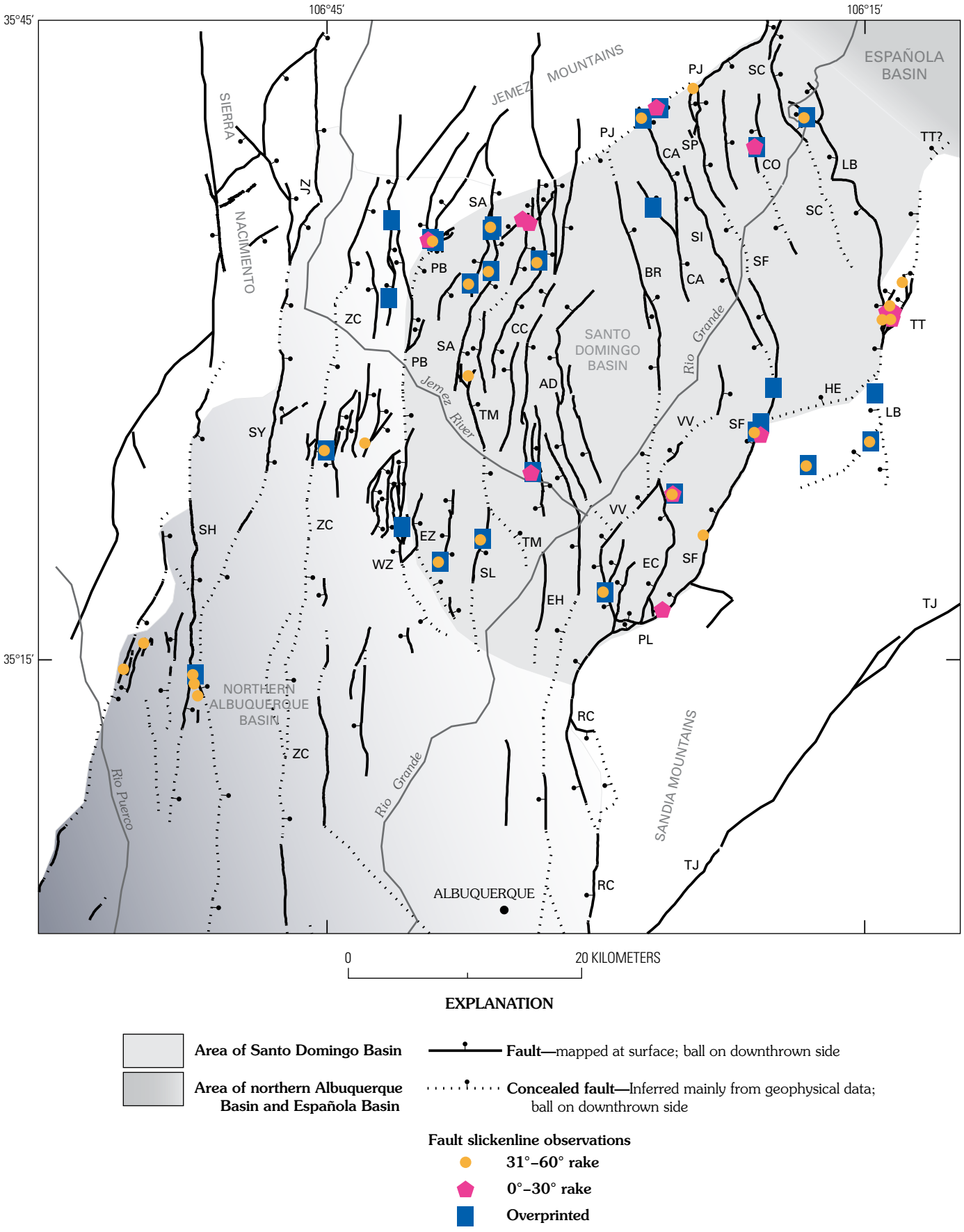

EXPLANATION

Area of Santo Domingo Basin

Area of northern Albuquerque Basin and Española Basin

Fault—mapped at surface; ball on downthrown side

Concealed fault—Inferred mainly from geophysical data; ball on downthrown side

Fault slickenline observations

31°–60° rake

0°–30° rake

Overprinted

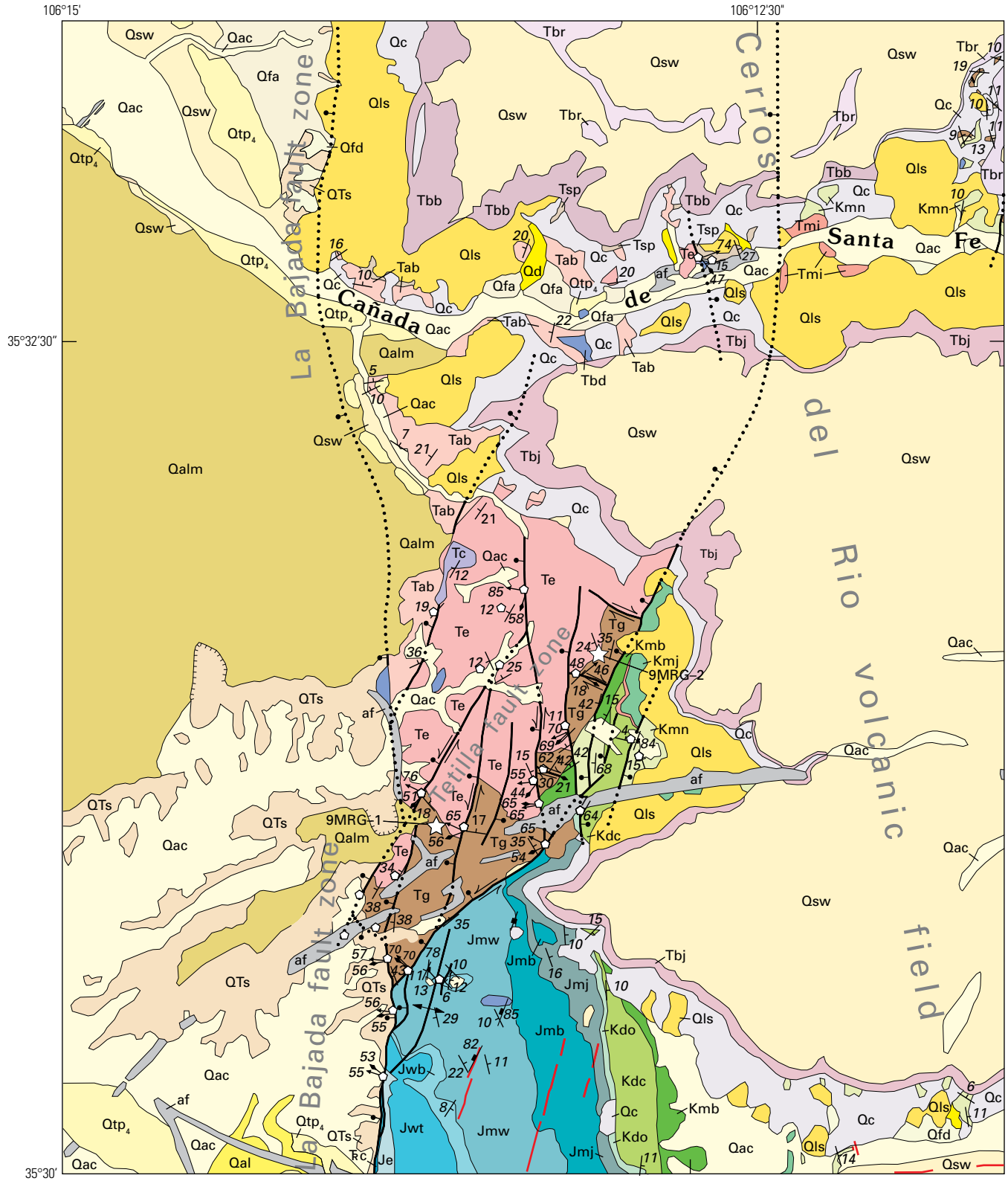

EXPLANATION

- **Fault**—Dotted where concealed; ball and bar on downthrown side; opposing arrows show sense of strike-slip component of movement; single barbed arrow shows direction and angle of dip; diamond arrow shows trend and rake of slickenlines
- **Anticline**
- **Basalt (Tbj?) dike**
- **Bedding**—Strike and dip
- **Joint**—Strike and dip
- **Fault-slip measurement site**
- **Paleomagnetic sample site**

0 1 KILOMETER

Figure E4 (facing page). Southwestern part of Tetilla Peak 7.5 minute quadrangle (from Sawyer and others, 2002) showing structural geometry of Tetilla fault zone where it is truncated by the younger La Bajada fault zone. Refer to plate 2 for explanation of map unit labels. Tetilla fault zone is constrained to be older than 2.7-Ma basaltic flows of the Cerros del Rio volcanic field (units Tbj, Tbb, Tbr) that overlap the northeast projection of the zone, whereas the younger La Bajada zone displaces similar 2.3-Ma flows about 500 m north of map area. Most faults within the Tetilla zone strike north-northeast; have down-to-west, normal-sinistral, oblique-slip displacement; and splay northward off a large-displacement fault bordering the east side of zone. Note small dextral-slip cross faults within exposed Tetilla zone.

Rift-border faulting migrated basinward to the north-striking, normal-slip La Bajada fault zone after 2.7 Ma. The prominent La Bajada fault zone extends along the base of the north-trending La Bajada escarpment; along it, 2.7-Ma early basalt flows of the Cerros del Rio volcanic field were dropped as much as 600 m basinward (pl. 6; fig. E4). Slip surfaces within this fault zone dip 50°–60° W. and possess normal-slip slickenlines (78°–86° S. rake) (fig. E5).

Geologic relations (chapter C, this volume) and electromagnetic data (chapter F, this volume) (fig. F12*A*–*C*) indicate that another northerly striking, possibly early rift-border fault (Cochiti Cone fault, pl. 2 (see also fig. E9)) is truncated by the La Bajada fault zone about 12 km north of the Tetilla fault zone. Small-displacement antithetic faults are also apparent just west of the Cochiti Cone fault as indicated by electromagnetic data (cross section A-A′, pl. 6). Geologic and geochronologic relations indicate that this down-to-basin fault was active during Cerros del Rio basaltic eruptions between 2.6 and 1.1 Ma, so it remained active somewhat later than the Tetilla zone before rift faulting in the area became restricted to the La Bajada and intrabasinal faults farther west.

Deformational Style of the Tetilla Fault Zone

Kinematic, magnetic, and paleomagnetic data from the Tetilla fault zone constrain the deformational style and history of this extensional transfer fault zone. Faults of the Tetilla zone possess normal-oblique–slip slickenlines (50°–75° S. rake); the larger displacement west-dipping faults have sinistral slip components, whereas the smaller east-dipping faults have dextral slip components (fig. E5). The Tetilla faults are generally steeply dipping (60°–90°), consistent with their strike slip components. The sinistral and dextral oblique slip on faults of opposing dip in the Tetilla zone is difficult to explain kinematically. One possible mechanism is opposing-sense rotation of fault blocks about moderately inclined axes owing to bulk sinistral transtension that accompanied lateral transfer of extension along the Tetilla paleorift boundary (fig. E6*A*) (Minor and Sawyer, 1999). Alternatively, northerly ramping that accompanied rift-flank uplift of rocks south of the Tetilla rift-border fault may have tilted original normal-slip faults northward, resulting in apparent sinistral and dextral oblique-slip slickenline orientations (fig. E6*B*). A third possibility is that the observed structural patterns resulted from a combination of the above two mechanisms.

To test for possible inclined-axis rotation associated with the strike-slip components of faulting in the Tetilla fault zone, magnetic fabrics and paleomagnetism of the Galisteo Formation were investigated at two sites. At site 9MRG–1 (see fig. E4 for location), 20 samples were collected from north-northeast-dipping sandstone and siltstone beds distributed through about 24 m of section. At site 9MRG–2, 18 samples were collected from 3 west-dipping sandstone intervals spaced at more or less equal intervals through about 50 m of section. Results of the magnetic and paleomagnetic investigations are summarized in table E1 and fig. E7.

Magnetic fabrics within the Galisteo Formation were investigated by using anisotropy of magnetic susceptibility (Hrouda, 1982). The principal axes of the minimum susceptibility (K3) for all samples are nearly perpendicular to bedding, as is typical for sedimentary rocks (fig. E7*A*). Axes of maximum susceptibility (K1) also cluster at each site; they trend north-northeast at site 9MRG–1 and northwest at site 9MRG–2. These axes lie at high angles to directions of Laramide shortening, and tentatively they are interpreted as intersection lineations between sedimentary and tectonic fabrics developed perpendicular to shortening (Housen and van der Pluijm, 1991).

Paleomagnetic analysis of Galisteo samples employed progressive thermal demagnetization to isolate characteristic remanent magnetization components. Remanent magnetization was unblocked at temperatures as high as 685°C, indicating that hematite was the principal carrier of the remanent magnetization in these red beds. For site 9MRG–1, remanent magnetization components mostly have south declinations and negative inclinations, indicating a reversed polarity (fig. E7*B*). One sample from the middle part of the section carries a normal-polarity remanent magnetization that is roughly antipodal to the reversed-polarity samples; the remanent magnetization direction for this sample was inverted to calculate the site mean direction. Analysis of five samples either did not isolate a single remanent magnetization component during demagnetization or isolated components that had directions that were intermediate between those of the reversed- and normal-polarity samples; these results were omitted from the site mean calculation. For site 9MRG–2, thermal demagnetization isolated well-defined, normal-polarity remanent magnetization in nearly all the samples (fig. E7*B*). Data from one sample that probably unblocked a mixture of normal- and reversed-polarity magnetization were omitted from the calculation of site mean direction.

The mean directions for the two sites became less similar after they were corrected for tilt, which suggests a negative fold test; the inclinations for the sites became more similar after they were corrected for tilt, and the difference between

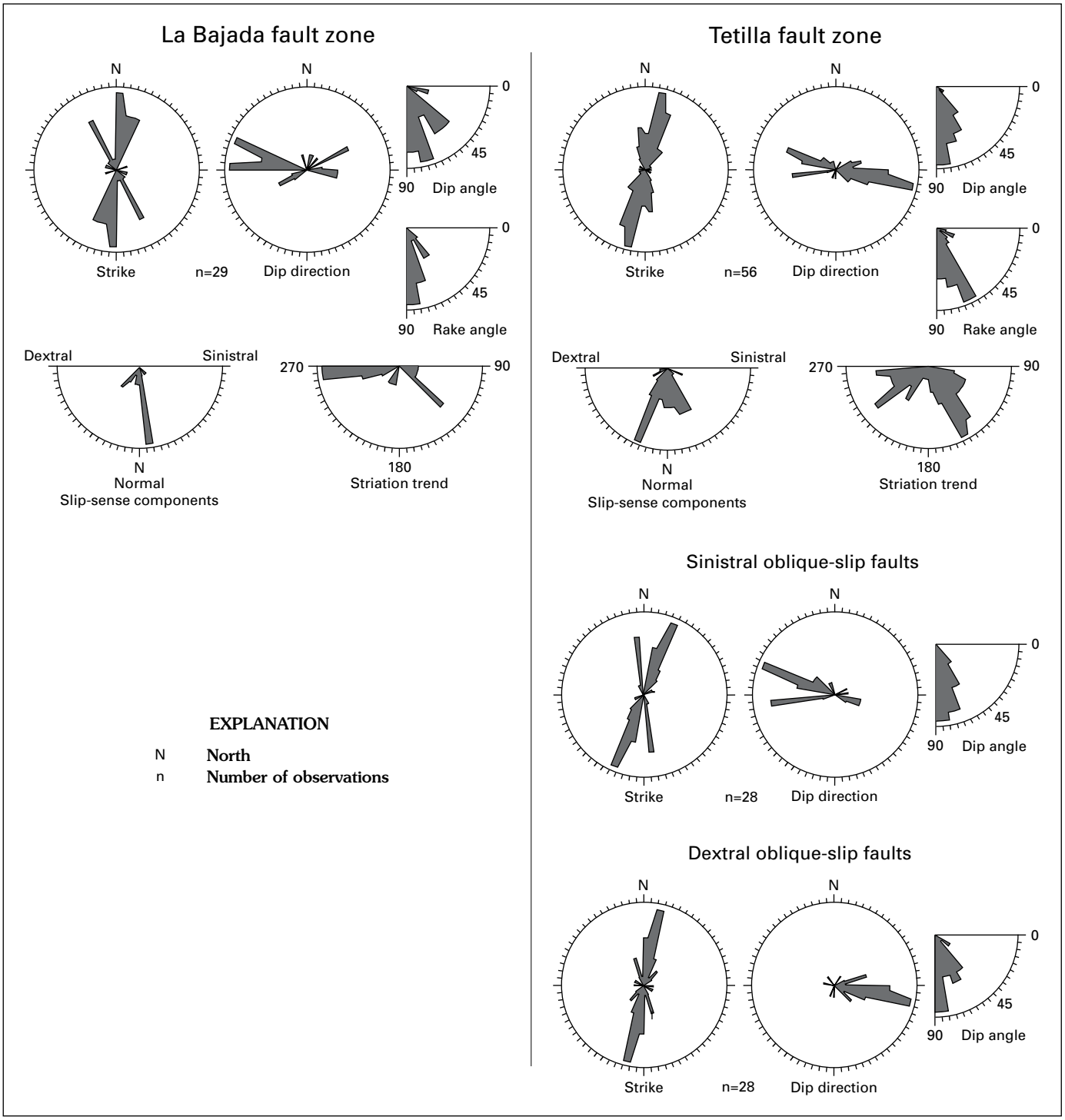

Figure E5. Orientation and kinematic attributes of fault-slip data collected within La Bajada and Tetilla fault zones. On slip-sense components diagrams, Dextral refers to pure dextral slip, Normal to pure normal slip, and Sinistral to pure sinistral slip. Most La Bajada faults dip 45°–80° W. and possess normal-slip slickenside striae (rake, 75°–90° S.). In comparison, Tetilla faults generally dip more steeply (60°–90°) and possess normal-oblique slip striae (rake, 60°–75° S.); west-dipping faults possess sinistral slip components whereas east-dipping faults possess dextral slip components.

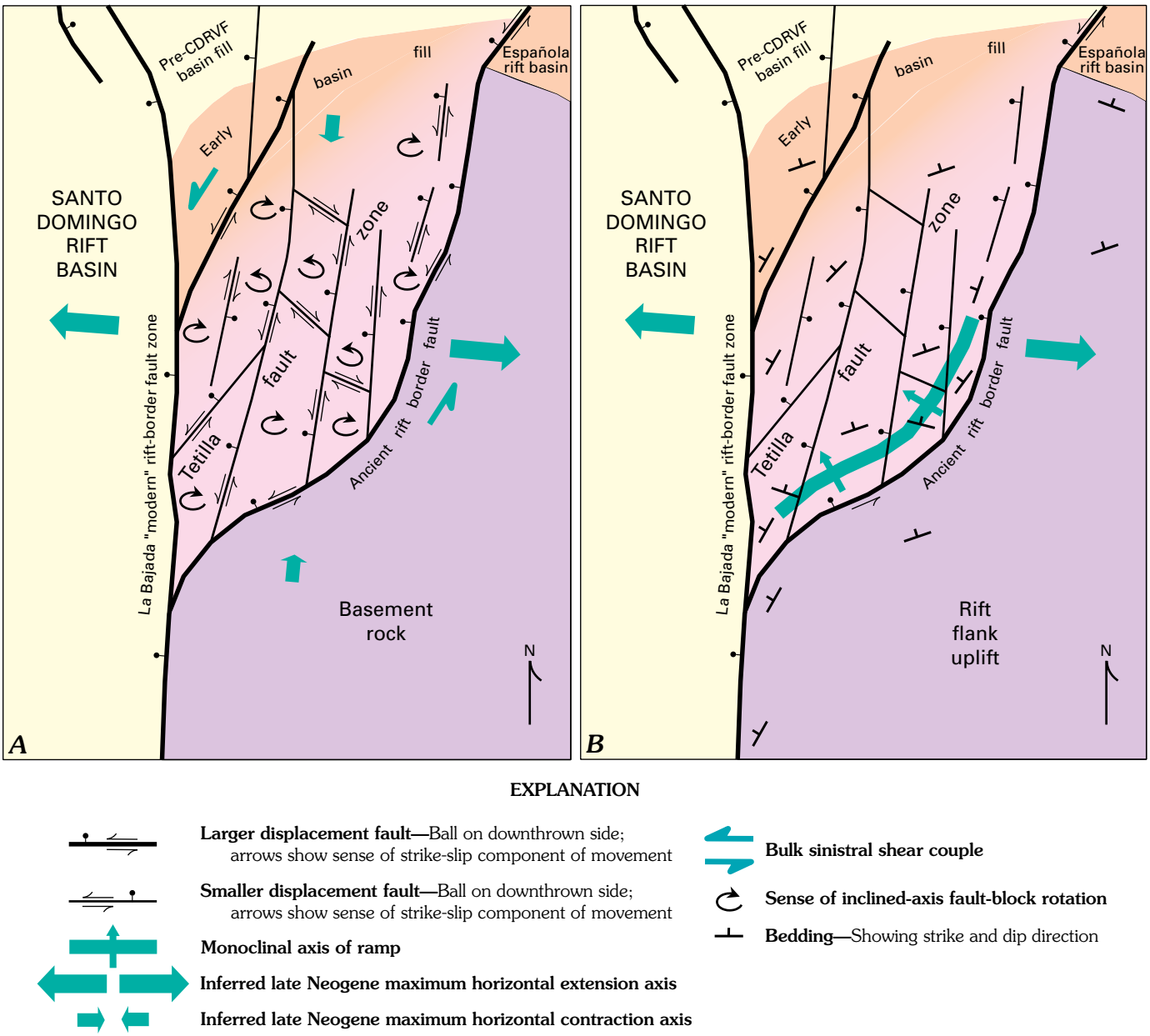

Figure E6. Two structural interpretations (A and B) of La Bajada and branching Tetilla fault zones based on structural and paleomagnetic data. See text for description of interpretations. The two interpretations differ in structural mechanisms invoked for Tetilla fault zone but not in interpreted temporal shift of rift-border faulting and structural role of the La Bajada zone. CDRVF, Cerros del Rio volcanic field.

the tilt-corrected directions is mostly in declination (fig. E7*B*). The difference in declinations of the remanent magnetizations is of the same sense and magnitude as for the declinations of the K1 axes. We interpret these declination differences to reflect differential vertical-axis rotation at the two sites (compare with fig. E7*A*, *B*).

By assuming that the remanent magnetizations carried by hematite were acquired as a chemical remanent magnetization soon after deposition of the Eocene Galisteo Formation, their declinations can be compared with expected directions calculated from magnetic poles of appropriate age from the North American apparent polar wander path (Besse and Courtillot, 1991) to quantify the absolute amount and sense of vertical-axis rotation. Compared with the declination of a 40-Ma expected direction, the vertical-axis rotation estimate at site 9MRG–1 is 19.1°±8.7° (clockwise) and at site 9MRG–2 is –36.6°±7.9° (counterclockwise) (fig. E7*B*). Compared with the expected direction, the inclinations of each site's mean direction after correction for tilt are shallow and statistically distinct at both sites (flattening at site 9MRG–1 is 33.3°±7.4° and at site 9MRG–2 is 17.0°±7.9°). At reversed-polarity site 9MRG–1, this flattening could reflect incomplete removal of a

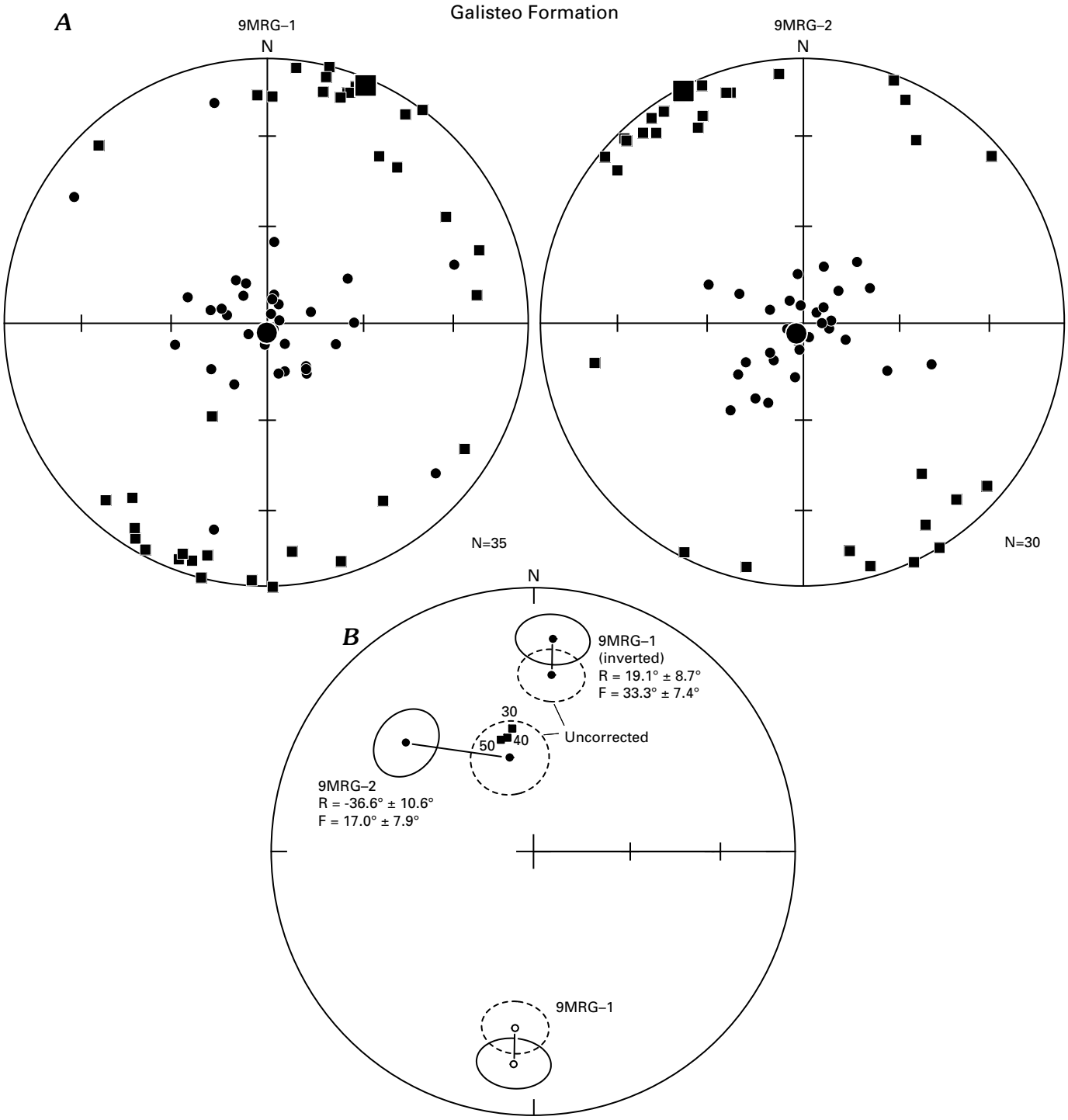

Figure E7. Rock magnetic data from samples of Eocene Galisteo Formation collected at sites 9MRG–1 and 9MRG–2 (see fig. E4 for locations) within Tetilla fault zone. Filled symbols are projections onto lower hemisphere and open symbols are projections onto upper hemisphere. *A*, Anisotropy of magnetic susceptibility data; squares and circles represent maximum and minimum principal axes of magnetic susceptibility ellipsoids, respectively. All directions are corrected for bedding dip. Small symbols are sample directions and large symbols are site-mean directions. *B*, Paleomagnetic site-mean directions before and after correction for bedding dip. Reversed-polarity site mean for 9MRG–1 is inverted through the origin for comparison with normal-polarity expected directions (squares) for the interval 50–30 Ma. For tilt-corrected site mean directions, rotation (R) and inclination flattening (F) parameters were calculated using methods of Demarest (1983) with reference to the 40-Ma expected direction.

Table E1. Rock magnetic data from Eocene Galisteo Formation, New Mexico.

[Latitude and Longitude referenced to 1927 North American datum; N/No, ratio of samples used in calculating the paleomagnetic site-mean directions to number of samples measured; Strike and Dip, tilt corrections in which dip direction 90° clockwise from strike direction; $Decl_0$, $Incl_0$, and $Decl_1$, $Incl_1$ are declination and inclination of the site-mean direction in uncorrected and tilt-corrected coordinates, respectively; R is the resultant vector; *k* is precision parameter (Fisher, 1953); and α_{95} is the radius of the cone of 95 percent confidence about the site-mean direction; $Decl_{K1}$, $Incl_{K1}$ and $Decl_{K3}$, $Incl_{K3}$ are declination and inclination of site-mean principle axes of maximum and minimum magnetic susceptibility, respectively, after tilt correction]

Site	Latitude (°N)	Longitude (°W)	N/No.	Strike (°)	Dip (°)	Dec_{I0} (°)	Inc_{I0} (°)	R	*k*	α95 (°)	$Decl_1$ (°)	$Incl_1$ (°)	$Decl_{K1}$ (°)	$Incl_{K1}$ (°)	$Decl_{K3}$ (°)	$Incl_{K3}$ (°)
9MRG–1	35.5181	106.2234	13/18	282	12	185.8	–33.3	12.4444	22	9.1	186.4	–21.0	22.6	3.1	183.1	87.1
9MRG–2	35.5279	106.2144	16/18	184	38	345.8	59.9	14.9447	14	10.1	310.5	36.6	332.5	1.3	214.8	86.2

normal polarity overprint, but incomplete removal would not explain the anomaly at site 9MRG–2. Most likely the inclination anomalies reflect deflection of the remanent magnetization during sedimentary compaction (Deamer and Kodama, 1990).

These results indicate local block rotations about steeply inclined axes, although the sense and amount of rotation was not uniform. Clockwise rotation (site 9MRG–1) is consistent with the sinistral components of slip recorded on down-to-basin faults (Freund, 1970). Counterclockwise rotation detected at site 9MRG–2 is unexpected given the preponderance of sinistral slip components within the Tetilla fault zone. However, the site is located within a local domain containing several dextral strike-slip cross faults that abut northerly striking sinistral-oblique faults (fig. E4). These and other dextral faults within the Tetilla fault zone may have accommodated local counterclockwise rotation (Freund, 1970).

The opposing-sense, inclined-axis rotations detected within the Tetilla fault zone are consistent with the proposed model that invokes transtension along the Tetilla paleorift boundary (fig. E6*A*). The opposing rotations suggest that bulk strain in the zone was more closely allied with pure shear than simple shear, perhaps owing to concurrent north-south contraction and east-west extension across the zone (fig. E6*A*). The existing data do not permit us to determine if rift-flank uplift and ramping (fig. E6*B*) also contributed to the Tetilla fault zone deformation.

Basinward Shift of Rift-Border Faulting

The geometry and evolution of rift-border faults along other parts of the Santo Domingo Basin margin resemble the Tetilla–La Bajada fault zone system, and we infer similar progressive spatial shifts of rift faulting on both sides of the basin. The east-northeast-striking Placitas fault zone (PL, figs. A2, E1), which forms part of the southeast border of the Santo Domingo Basin, is an oblique-slip transfer fault zone that links the Rincon (RC) and San Francisco (SF) border faults (Connell and others, 1995; Karlstrom and others, 1999). The Placitas zone is similar to the Tetilla fault zone in that north-striking, mainly down-to-basin, normal and oblique-normal faults abut its north side (fig. E3) and northward stratal dips exist within and adjacent to the zone (Connell and others, 1995). Karlstrom and others (1999) inferred that northward stratal tilting in the area mostly resulted from Neogene extensional uplift of the Sandia Mountains, and they invoked Laramide and younger changes in the principal strain axes to explain the complex oblique-slip and strike-slip slickenlines on individual faults in the Placitas zone. They also inferred that the Placitas fault zone and southern San Francisco fault are inactive, and they viewed northern extensions of the Rincon fault—including the Valley View (VV) fault—as the more recently active basin-bounding structures (see also the northern La Bajada fault zone (LB)) (figs. A2, E1).

The Hagan Embagment fault (HE), northeast of the Placitas area (figs. A2, E1), is probably an analogous extinct transfer fault zone that relayed extensional strain to the southern La Bajada fault zone (LB) before activity became restricted to the northern San Francisco fault (SF). Young displacement along the San Francisco fault north of the Hagan Embagment fault intersection is indicated by its offset of the 1.61-Ma lower part of the Bandelier Tuff (Smith and Kuhle, 1998; Smith, McIntosh, and Kuhle, 2001). Kelley (1977) similarly inferred that both the northern San Francisco fault and the Rincon fault south of Placitas are relatively young "bench" faults that had moved more recently than the Tijeras (TJ)–southern La Bajada (LB) "back-bench" fault zones to the east. The youthful geomorphology of the Sandia Mountains block was cited by Kelley (1977) as evidence of recent uplift along the Rincon fault.

Thus, structural and geomorphic evidence indicates that the active eastern borders of both the Santo Domingo and northern Albuquerque Basins shifted west-northwest, towards the rift axis, as the basins developed in the Neogene (fig. E8). The most recently active border faults, such as the northern La Bajada and northern San Francisco faults, are probably long-lived growth faults that were active within the basin interiors early in their histories. Evidence of growth-fault relations along faults within the Albuquerque and Santo Domingo Basins is provided by gravity, seismic, and drill-hole data indicating abrupt stratigraphic thickening on the downthrown sides of faults (Russell and Snelson, 1994). Also, the nature of aeromagnetic anomalies along intrabasinal faults (fig. D5) are consistent with growth-fault structural and stratigraphic geometries (Grauch, Hudson, and Minor, 2001; chapter D, this volume).

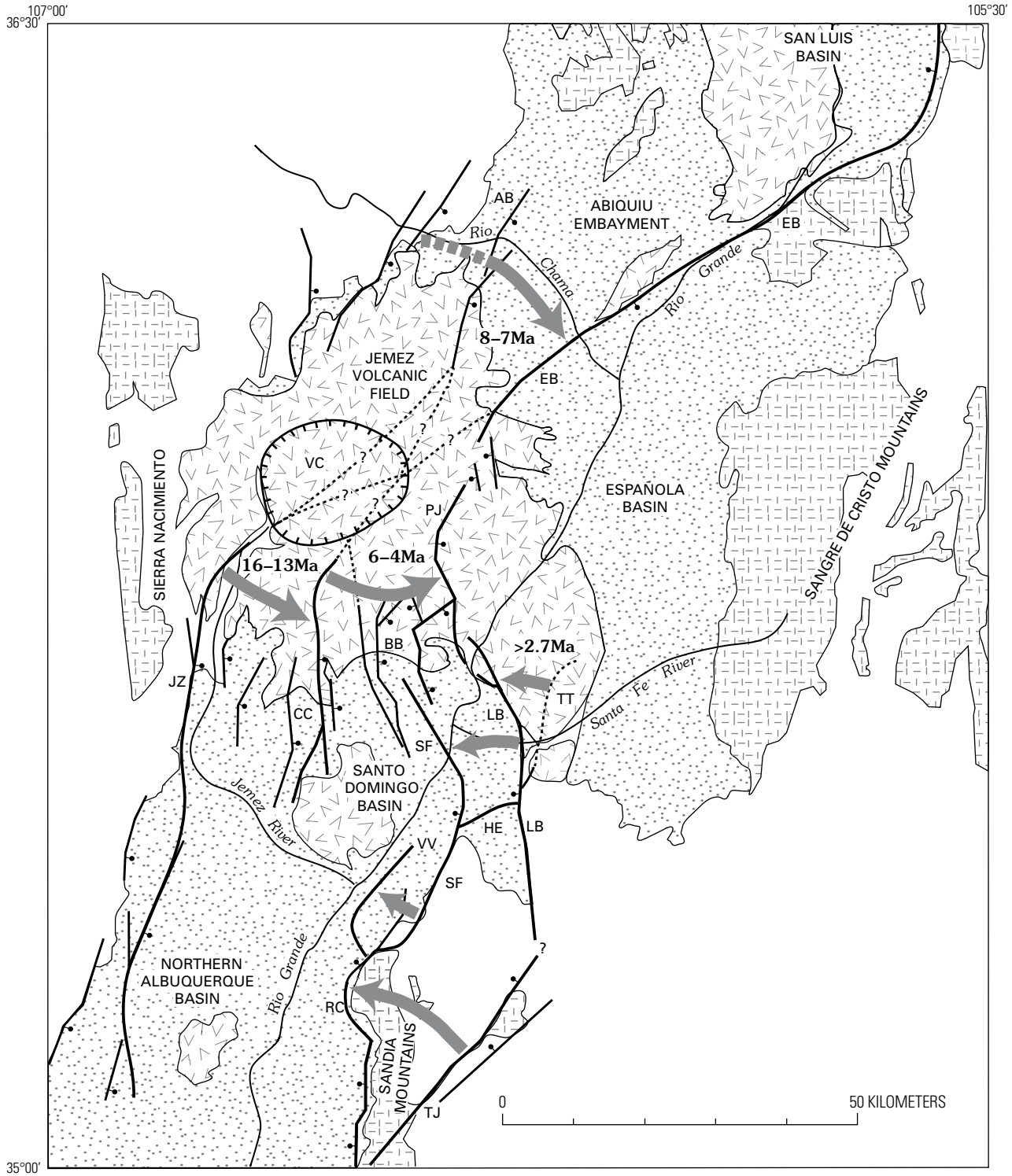

EXPLANATION

- **Pleistocene–Miocene volcanic rocks**
- **Pleistocene–Oligocene basin-fill sediment**
- **Lower Oligocene–Paleozoic rocks**
- **Precambrian rocks**
- **Active or once-active rift border fault—**Bar and ball on downthrown side; dotted where concealed; queried where uncertain
- **Other fault—**Bar and ball on downthrown side
- **Caldera boundry**
- **Migration direction of active rift border faulting—**Dashed where uncertain

Figure E8 (facing page). Northern Albuquerque, Santo Domingo, and Española Basins, showing migration patterns (curved gray arrows) and timing of active rift-border faulting. See text for discussion. Border faults delineated by thick black lines. Modified from Smith, McIntosh, and Kuhle (2001). VC, Valles caldera. Faults and fault zones: AB, Abiquiu, BB, Bearhead Basin; CC, Cañada de Cochiti; EB, Embudo; HE, Hagan Embayment; JZ, Jemez; LB, La Bajada; PJ, Pajarito; RC, Rincon; SF, San Francisco; TJ, Tijeras; TT, Tetilla; VV, Valley View.

Evidence of basinward shifts of rift-border faults on the northwest side of the Santo Domingo Basin and on the west side of the Española Basin was reported by several workers (Gardner and Goff, 1984; Aldrich, 1986; Baldridge and others, 1994). Gardner and Goff (1984) and Aldrich (1986) suggested that the Neogene active structural margin of the rift migrated progressively eastward from the northern Jemez fault (JZ, figs. A2, E1, E8) to the Cañada de Cochiti fault (CC), and finally (about 5 Ma) to the Pajarito fault (PJ) along the edge of the modern Española Basin. The first two fault zones are inferred to have projected to the northeast and linked with northwestern border faults of the Española Basin (Embudo fault zone (EB)) prior to burial by Neogene deposits of the Jemez volcanic field and subsequent collapse of the Valles caldera (VC, fig. E8). The Pajarito fault astride the Saint Peters Dome block (fig. A2) may have formed as early as the late Oligocene and probably remained active while the Española Basin was subsiding (Cather, 1992), whereas down-to-east fault zones farther west, such as the Cañada de Cochiti zone, probably became extinct late in the Miocene.

On the north side of the Jemez volcanic field in the lower Rio Chama area, Baldridge and others (1994) inferred similar abandonment and eastward shift of border faulting toward the axis of the Española Basin. They determined that border faulting in the Abiquiu embayment ended between 8 and 7 Ma and migrated basinward to the Embudo fault zone (EB, fig. E8) (Baldridge and others, 1994). The northeast-striking older Abiquiu border faults (AB) are roughly aligned with the older border faults just south of the Valles caldera (JZ, CC), suggesting that both sets of faults may have once been part of a continuous border fault zone before Jemez volcanism (dotted queried faults, fig. E8).

The inward migration of active border faulting on both sides of the basins suggests that the zone of active rifting progressively narrowed during the Neogene (fig. E8). Faults in the axial parts of the rift basins may have been active for the greatest period of time and may have the most continuous and complete growth-fault histories, whereas toward the margins faults may have gone extinct at progressively earlier times. A similar pattern of faults younging toward the rift axis could alternatively be explained by a fixed-width axial zone of active faulting coupled with rift-normal extension that resulted in outward movement of fault blocks. In such a scenario faults would have become extinct once they moved outside the zone of active rift faulting. However, the cumulative amount of Miocene and younger crustal extension owed to rifting in the region is too small, only about 14 percent across the northern Albuquerque Basin (Woodward, 1977), to fully explain the abandonment of outer rift-border faults. Thus, we view rift narrowing as the chief cause of the observed faulting patterns. Baldridge and others (1994) came to a similar conclusion on the basis of their fault-timing observations on the northwest side of the Española Basin. We suggest that rift narrowing may be due to localization of strain within the crust. In this process rift-related extension occurs in a progressively narrower zone of faults in response to increasingly localized lithospheric necking (Buck, Lavier, and Poliakov, 1999) or to cooling along the rift axis.

Our interpretation differs from that of Kelley (1977), who inferred that a series of narrow central grabens formed first and that the basins got wider with time as rift faulting expanded outward. Kelley's model was based on inferred uplift and erosional stripping of pre-rift Cretaceous and Eocene deposits on the flanks of the early rift and coeval preservation of these deposits within narrow central troughs owing to early trough subsidence. However, this irregular distribution of pre-rift deposits can instead be attributed to localized Laramide structural and depositional patterns (Cather, 1992).

Structural Development of Santo Domingo Basin

To summarize, the salient structural attributes of the Santo Domingo Basin are (1) a northeast basin elongation defined by a large, gravity-expressed, oval, deep (>3 km) inner basin that is flanked along its longer margins by northeast-striking, partly buried, down-to-basin faults; (2) crudely semicircular, concentrically arranged, mostly down-to-basin, normal-slip faults that commonly curve into or offset the northeast-striking border faults on the northwest and southeast sides of the basin; (3) the common presence of late dextral and sinistral oblique-slip and strike-slip fault slickenlines that are interspersed in the longer, northeast-trending, margins of the basin; (4) at the southern and northeastern ends of the basin, interleaved or overlapping faults of opposing dip that project into the basin from opposite sides but which die out along strike and thus do not provide complete structural closure of the basin; and (5) outer limits of active border faulting that appear to have migrated basinward during rifting and abandoned faults on the flanks of the rift whereas inner basin-margin faults remained active throughout longer time spans and acquired more pronounced growth-fault geometries.

Given these observations, we infer that early structural development of the Santo Domingo Basin was dominated by oblique-normal rifting along northeast-striking faults. These early fault trends may have been inherited from northeast-striking Proterozoic shear zones that have been recognized in basement rocks regionally (Karlstrom and others, 1999). Along the rift margins large northeast-striking faults (such as the San Francisco (SF) and Pajarito (PJ) faults, fig. A2)

likely propagated northeastward and southwestward from the northern Albuquerque and southwestern Española Basins, respectively. An intrabasinal network of semicircular faults began to develop soon after establishment of northeast-striking basin-margin faults, presumably to accommodate intrarift, roughly east-west, extension concentrated in the area of the eventual basin depocenter. Many of these concentric faults merged with, curved into, or otherwise used the northeast fault trends, suggesting that the two fault systems eventually evolved into a single kinematically coordinated system. As rifting, basin subsidence, and deposition proceeded, displacement continued or increased on intrabasin, northerly striking, faults and fault segments and on inner-margin, northeast-striking faults, whereas fault movement diminished on the outer flanks of the basin. Thus, rift-related faulting became increasingly centered and spatially confined near the Santo Domingo Basin depocenter (shaded star on fig. E1).

The northeast-striking faults flanking the Santo Domingo Basin likely served as oblique transfer faults (Faulds and Varga, 1998) that accommodated and transferred rift-related extensional strain between the Española and northern Albuquerque Basins (figs. A2, E1) (Kelly, 1977, 1982; Chamberlin, 1999; Karlstrom and others, 1999; Minor and Sawyer, 1999). Early sinistral-oblique slip indicators are expected on most of these faults, if one assumes that the regional maximum extension and minimum horizontal stress directions were east-west to west-northwest–east-southeast (Woodward, 1977; Aldrich, Chapin, and Laughlin, 1986) during the early tectonic history of the Santo Domingo Basin. However, slip data from basin-margin faults indicate that strain was complex, involving normal slip and younger sinistral as well as dextral slip on faults having a variety of orientations. Although poorly understood, such fault-related strain probably reflects localized rotation of fault blocks or principal stress trajectories caused by concentrated lateral shear, which was itself caused by large extensional strain gradients along the basin margins. The dominantly normal-slip character of northerly striking semicircular faults in the central part of the basin suggests that away from the basin margins, faults formed in more favorable orientations with respect to the regional stress field, extensional strain was relatively uniform, and thus lateral shear was diminished.

Given the unique symmetrical structural geometry of the Santo Domingo Basin and its apparent structural linkages to the adjacent rift basins, Smith, McIntosh, and Kuhle (2001), following Faulds and Varga (1998), viewed the entire basin as a broad antithetic, anticlinal, strike-parallel accommodation zone linking the opposing northern Albuquerque and Española half-graben basins. We adopt this structural interpretation of the Santo Domingo Basin and, furthermore, suggest that the overall semicircular fault pattern partly resulted from the mechanical interaction and interference of overlapping, oppositely dipping faults that propagated and splayed northward and southward into the basin from as far as the margins of the adjoining basins.

Structural Geology of La Bajada Constriction

Structural Symmetry

The La Bajada constriction area in the northeast part of the Santo Domingo Basin possesses a structural symmetry that reflects overlapping structural elements inherited from the Española Basin and northern Albuquerque Basin (fig. A2) (Smith, McIntosh, and Kuhle, 2001). This area has a north-northwest-trending structural grain that is imparted by interleaved down-to-east and down-to-west faults (pl. 2, fig. E9). Down-to-west faults (La Bajada and San Francisco fault zones) are most common east of the Rio Grande and increase in throw towards the south, whereas faults with opposite throw and displacement gradients prevail west of the Rio Grande (such as South Pajarito and Camada faults) (fig. E9). Along the northwest side of the La Bajada constriction, surface traces of several of the larger intrabasin faults abut, curve into, or end just south of the northeast-striking Pajarito border fault zone. In the southeast part of the constriction, concealed but aeromagnetically expressed intrabasin faults apparently terminate well short of the La Bajada fault zone (pl. 2, fig. E9). Thus, basin-fill deposits in the northeast part of the constriction may have some structural connection with similar deposits to the southwest, which may facilitate downgradient flow of ground water through the constriction (see chapter G, this volume, for further discussion of this topic).

Smith, McIntosh, and Kuhle (2001) described antiformal (opposing) stratal dips in the northeast part of the Santo Domingo Basin, which is expressed by gentle (≤15°) east dips east of the Cochiti graben and gentle west dips west of the graben (cross sections A-A′, B-B′, and F-F″, pl. 6; fig. E9). The axial Cochiti graben is bounded by the opposite-dipping South Pajarito and Cochiti faults and contains gently dipping beds cut by a graben-parallel, small-displacement fault. South of the graben the antiform axis steps westward and is expressed by relatively abrupt reversals in stratal dip across the Camada fault (sections C-C′ and D-D′, pl. 6; fig. E9) (Smith, McIntosh, and Kuhle, 2001). In general, stratal dips are greatest in fault blocks directly adjacent to the antiform axis (or Cochiti graben) and gradually decrease towards the east and west margins of the basin (pl. 6; fig. E9).

Figure E9 (facing page). La Bajada constriction area showing structural configuration of intrabasin areas and basin borders. Gray background shading shows topography of area. North-northwest structural grain of basin interior is oblique to northeast trend of La Bajada constriction and basin-border faults (such as the Pajarito fault). Interleaved intrabasin faults displace sediments down both to southwest and northeast.

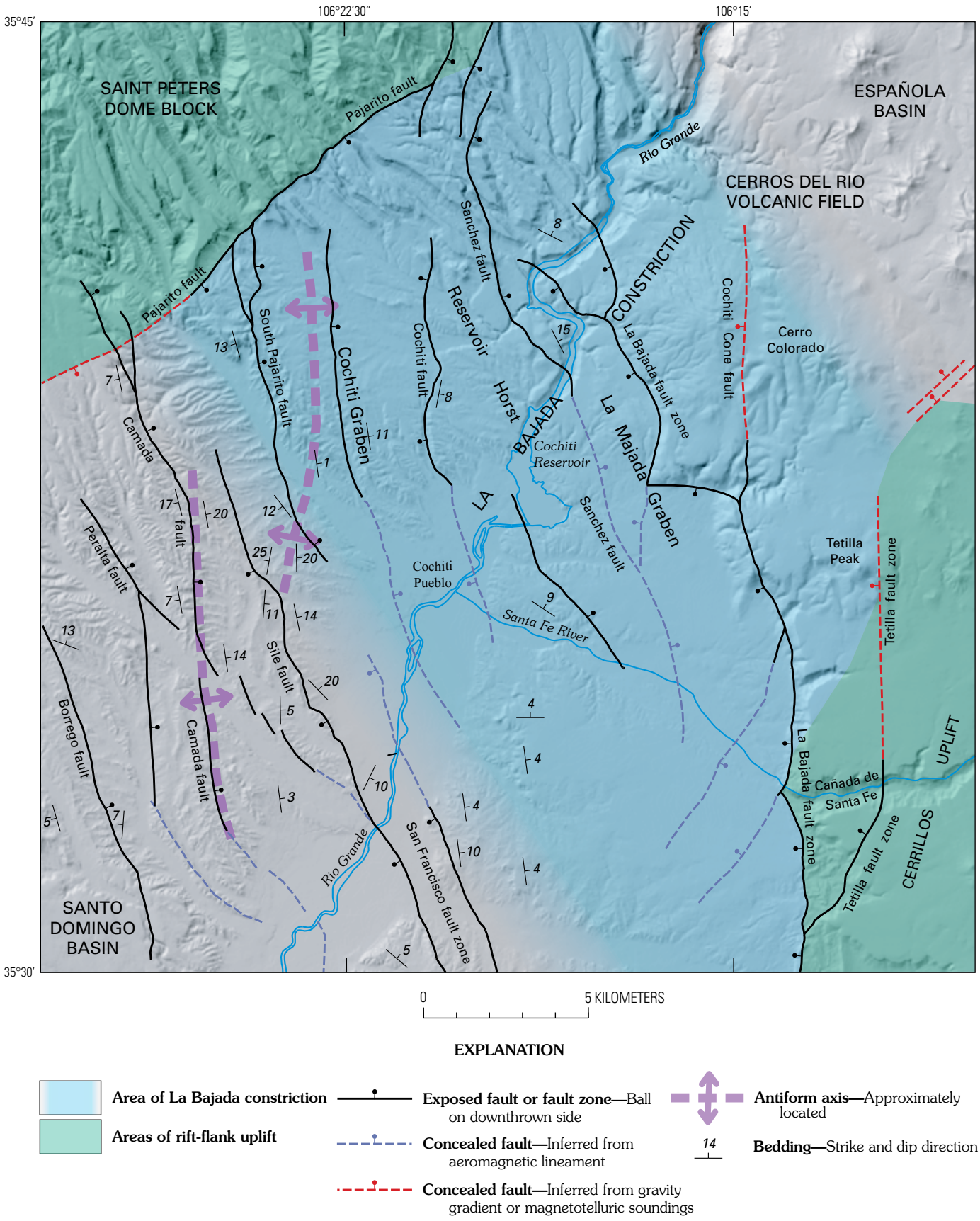

EXPLANATION

- **Area of La Bajada constriction**
- **Areas of rift-flank uplift**
- **Exposed fault or fault zone**—Ball on downthrown side
- **Concealed fault**—Inferred from aeromagnetic lineament
- **Concealed fault**—Inferred from gravity gradient or magnetotelluric soundings
- **Antiform axis**—Approximately located
- **Bedding**—Strike and dip direction

East of the Cochiti graben and adjacent Reservoir horst is the narrower and possibly younger La Majada graben, which is bounded by basinward-hooking strands of the La Bajada fault zone and the opposite-dipping Sanchez fault (figs. E9, E10). Although not antiformal, the northern part of this graben, where the La Bajada fault zone converges and dies out toward the adjacent Sanchez fault, may represent the youngest in a series of segmented, right-stepping, faulted antiforms or grabens that track northeastward migration of the rift axis (see discussion in next section). Latest movement on the northern La Majada graben faults (that is, northern La Bajada and Sanchez faults, fig. E9) postdates eruption of the 1.14-Ma basaltic andesite of Cochiti Cone (unit Qcc, pl. 2) and possibly follows deposition of the 55-ka El Cajete tephra (unit Qec, pl. 2) (chapter G, this volume).

The structural symmetry and rift history described above generally support the tectonic model of Smith, McIntosh, and Kuhle (2001). They inferred a complex pattern of back-and-forth, "seesaw" subsidence and tilting in the northeast part of the Santo Domingo Basin, including the La Bajada constriction area, in which the locus of normal-fault activity alternated between sides of the basin. As a refinement to the "seesaw" model, we suggest that subsidence within the Santo Domingo Basin was accommodated by faults propagating simultaneously southward and northward from, respectively, the Española and northern Albuquerque Basins. We infer that basin-margin faulting also shifted towards the basin axis as rifting proceeded, resulting in a narrowing zone of active rifting. Within the La Bajada constriction area, basin-axis faulting apparently stepped progressively right, or northeast, toward the narrowest part of the constriction and the young northern La Majada graben (fig. E9).

Sanchez and Northern La Bajada Fault Zones

The northern La Bajada fault zone and nearby Sanchez fault are discussed in detail in this section to elucidate the structural evolution and configuration of this important narrow part of the La Bajada constriction. The La Bajada fault zone strikes northward from where it crosses the older Tetilla fault zone for about 10 km and then curves to the northwest and terminates near the opposite-dipping Sanchez fault (pl. 2, figs. E9, E10). The Sanchez fault is here defined as the south-southeast-striking, down-to-east fault that approaches and nearly merges with the Pajarito fault zone where it bends prominently near Saint Peters Dome (pl. 2, fig. E9). On the basis of aeromagnetic data, the Sanchez fault (SC) appears to project southward beyond the Rio Grande for at least 10 km parallel to the La Bajada fault zone (pl. 2, fig. D7). The northern La Bajada fault zone along its overlap with the Sanchez fault is characterized by scalloped traces and oblique slip (fig. E10). The La Bajada fault zone bifurcates near the Rio Grande into splays that hook towards the Sanchez fault (fig. E10). Both splays terminate short of the Sanchez fault, but because the two fault systems dip toward each other they may intersect at shallow depth. The scalloped and hooked geometry of the northern La Bajada fault zone suggests that this part of the fault zone evolved by mechanical interaction and linkage of originally left-stepping en echelon fault segments (Olson and Pollard, 1989; Childs, Watterson, and Walsh, 1995; Acocella, Gudmundsson, and Funiciello, 2000). The hooking of the La Bajada fault zone splays towards the nearby Sanchez fault (fig. E10) suggests that there also has been mechanical interaction between these two fault zones. The scalloped, segmented geometry of the La Bajada fault zone traces and the fact that this part of the fault zone offsets units as young as the 1.14-Ma basaltic andesite of Cochiti Cone (unit Qcc, pl. 2) suggest that the northern part of the fault zone is relatively youthful and structurally immature (Acocella, Gudmundsson, and Funiciello, 2000).

Fault kinematic indicators reveal that most intrabasin faults in the La Bajada constriction area have undergone normal slip (rakes >60°). Similar to indicators in the rest of the basin, oblique-slip and, rarely, strike-slip indicators are observed only locally on faults on the northwest and southeast margins of the constriction (Tetilla (TT) and Pajarito (PJ) fault zones, fig. E3). The left-stepping en echelon traces of the intrabasin Sile fault (fig. E9) and the discontinuous, poorly exposed fault on the northeast side of Cañon Santo Domingo (pls. 1, 2) suggest that oblique slip occurred along those faults. However, only normal-slip indicators are observed on the Sile fault, and most intrabasin faults in the La Bajada constriction area have relatively straight traces that lack direct evidence of pronounced oblique slip. The normal-slip nature of faults within the La Bajada constriction implies that during faulting the horizontal maximum extension direction in this part of the basin was oriented approximately southwest, towards the Santo Domingo Basin depocenter (shaded star, fig. E1).

Hydrogeologic Character of Santo Domingo Basin Faults

Structural properties and cement patterns of fault zones within the Santo Domingo Basin and northern Albuquerque Basin have been investigated by two of the authors (Minor and Hudson, 2006) to facilitate hydrogeologic characterization and modeling of faults in the Albuquerque Basin aquifer. Results of that study that bear on the hydrogeologic properties of faults in the Santo Domingo Basin and, in particular, the La Bajada constriction are summarized below. Implications of the constriction fault geometry on ground-water flow are discussed in chapter G of this volume.

Fault Zone Structure and Hydrogeology

A typical fault zone in the Santo Domingo Basin area has three structural components: (1) a central fault core consisting of a narrow zone of concentrated shear strain, attenuation, and local grain-size reduction; (2) adjacent mixed zones composed of transitional domains of bedding disruption, entrainment, and localized particulate flow; and

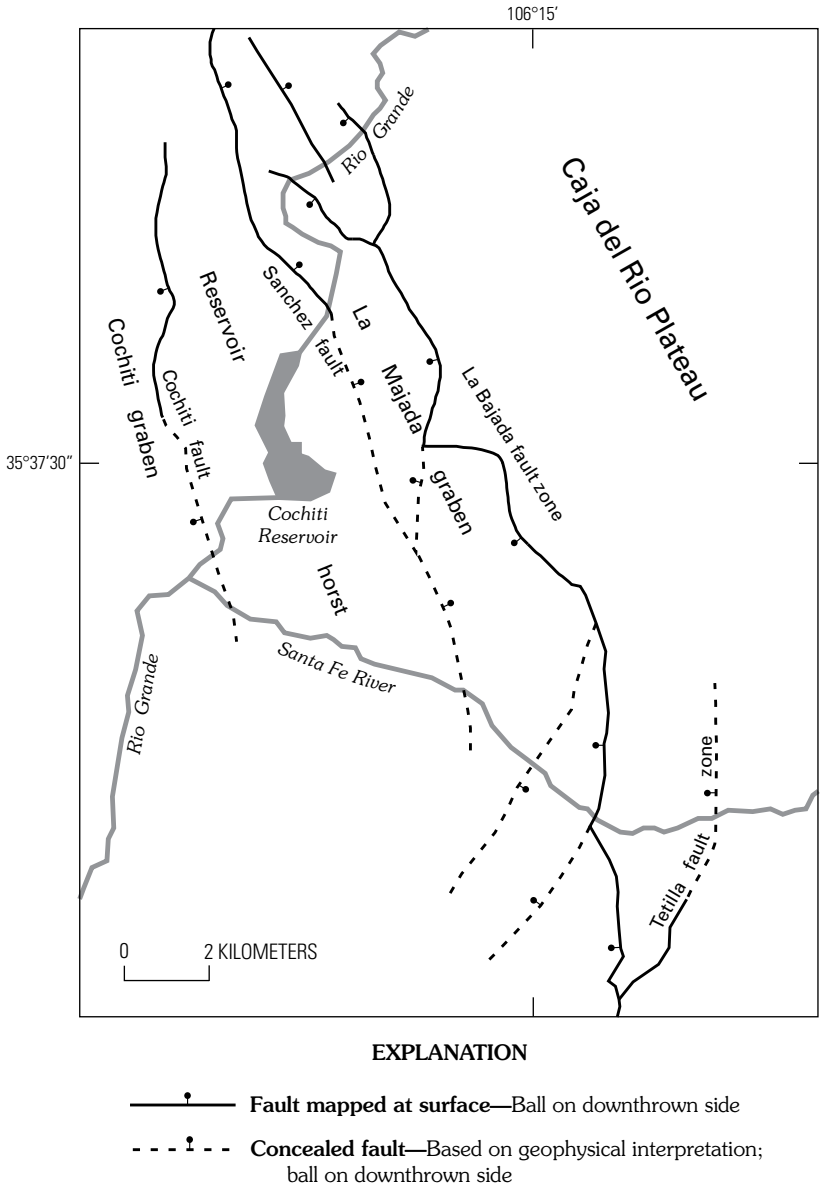

Figure E10. Inward hooking and scalloped traces of northernmost La Bajada fault zone where it overlaps with opposite-displacement Sanchez fault. Peculiar La Bajada fault zone geometry is attributed to mechanical interaction and linkage of en echelon fault segments as well as interaction of La Bajada fault with Sanchez fault. See text for further discussion. Faults shown as mapped at surface based on plate 2 and Sawyer and others (2002); concealed fault segments based on geophysical interpretations presented in chapter D (this volume).

(3) outer damage zones consisting of tabular rock volumes containing subsidiary faults, fractures, deformation bands, veins, and drag folds that decrease in intensity outwards (fig. E11). This structural architecture is consistent with fault zone observations in the Albuquerque Basin (Heynekamp and others, 1999; Rawling, Goodwin, and Wilson, 2001). Sheared and foliated clay-rich cores are common in nearly all faulted protoliths within the northeastern part of the Santo Domingo Basin. Clays within the cores appear to be derived from fault-entrained clay-bearing clastic protoliths (Caine, Evans, and Forster, 2004). Fault cores also contain variable amounts of silt, sand, and more rarely pebbles where faults cut coarser grained facies of the Sierra Ladrones (units QTsa, QTsp, pl. 2) and Cochiti (unit QTc) Formations. Sheared, brecciated, and comminuted volcanic rock cores are concentrated along the northern and northeastern margins of the basin where tuffs and lavas of the Jemez and Cerros del Rio volcanic fields are prevalent. Given the fine-grained clay-rich nature of a large majority of fault cores in a variety of protoliths, it is likely that most of the cores have very low permeability, especially in directions normal to the fault core (Knipe, 1993; Caine, Evans, and Forster, 1996; Caine and Forster, 1999; Heynekamp and others, 1999; Rawling, Goodwin, and Wilson, 2001; Caine, Evans, and Forster, 2002). Thus, despite their relatively narrow widths (mean of 0.1 m compared with ~10 m for damage zones), continuous undisturbed cores should act as important seals to across-fault fluid flow and contribute to anisotropic permeability within intrabasin fault zones (Knipe, 1993; Caine and Forster, 1999; Rawling, Goodwin, and Wilson, 2001; Caine, Evans, and Forster, 2002).

Variations in the protolith, especially grain size, affect observed fault zone properties. The width of a fault zone generally increases with decreasing grain size in sedimentary protoliths, but a large proportion of the narrowest fault zone components is in or adjacent to protoliths rich in clay (or mudstone) and silt (or siltstone). Most of the widest fault zones are in well-lithified volcanic rocks and other similar, well-indurated protoliths, whereas relatively narrow fault zone components tend to be hosted by protoliths rich in gravel, such as those within axial-river facies of the Sierra Ladrones Formation (unit QTsa, pl. 2; chapter B, this volume). These preliminary correlations of fault-zone properties and protolith suggest that knowledge of major subsurface lithostratigraphic changes in the basin can be used to help predict downdip variations in fault zone widths and width-dependant hydrologic properties.

Four main categories of fractures are recognized in fault damage zones in the study area: (1) opening-mode, or extension, fractures, (2) synthetic mesoscale shear fractures (that is, faults) and deformation bands, (3) antithetic mesoscale shear fractures and deformation bands, and (4) cross, or oblique, fractures (fig. E11). Zones of breccia are also present locally. Fault zones in relatively lithified and indurated volcanic and sedimentary protoliths, which are concentrated along the northern and eastern margins of the Santo Domingo Basin, are most likely to have open, hydraulically conductive shear and extension fractures within their damage zones (Caine, Evans, and Forster, 1996). In contrast, intrabasin fault damage zones in poorly to moderately consolidated sediments of the Santa Fe Group commonly contain low-permeability deformation bands (Heynekamp and others, 1999; Rawling,

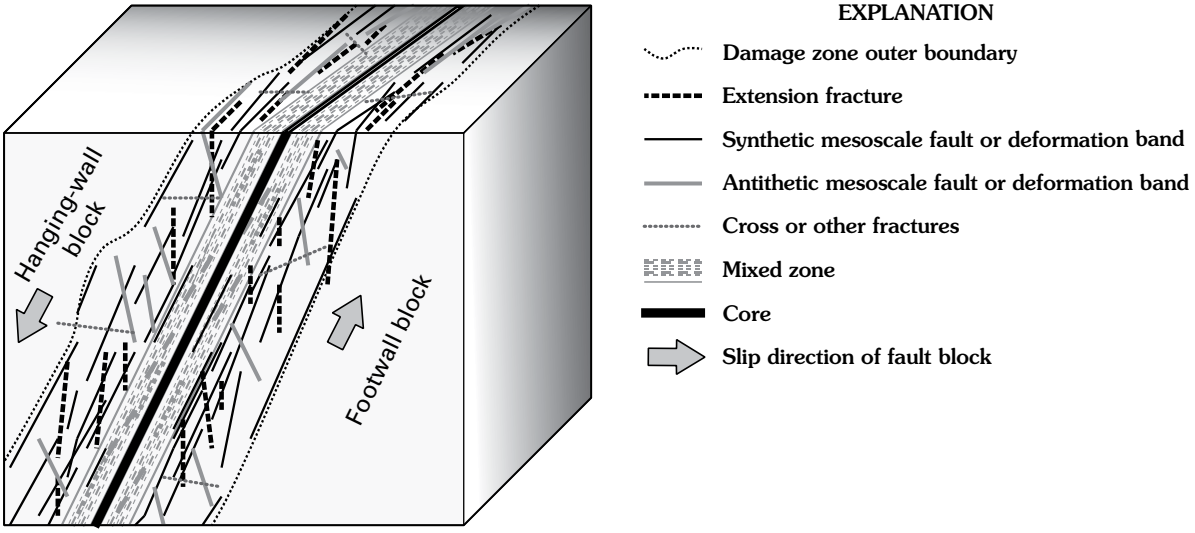

Figure E11. Various architectural components and damage zone fracture types observed in faults exposed in studied basins. See discussion in text.

Goodwin, and Wilson, 2001) as well as variable-permeability open-to-closed shear fractures and rare extension fractures. Damage zones dominated by uncemented extension fractures and synthetic and antithetic shear fractures have enhanced permeability in directions approximately parallel to the principal fault plane or core (Sibson, 1996; Caine and Forster, 1999). As the density of deformation bands in damage zones increases, as is commonly the case in faults cutting basin-fill sediments, bulk fault-zone permeability and especially fault-normal permeability typically decrease (Rawling, Goodwin, and Wilson, 2001). Regardless of the structural composition of the damage zones, most fault zones in the Santo Domingo Basin should retard or restrict across-fault ground-water flow owing to the combined effect of low-permeability damage-zone structures and very low permeability clay-rich cores.

Fault Zone Cement Patterns

The permeability of fault zones is substantially reduced where they are cemented and, thus, faults can evolve from zones of high permeability to zones of low permeability (Knipe, 1993; Mozley and Goodwin, 1995; Caine and Forster, 1999). If we assume that fault zone cements are indicators of focused flow of ancient fluid (Knipe, 1993; Mozley and Goodwin, 1995; Caine and Forster, 1999), then the spatial distribution of fault zone cements across a faulted aquifer basin can be used to identify areas of concentrated flow of ancient ground water.

Fault-zone cement is common in the Santo Domingo Basin, particularly where fault zones are rich in gravel or sand. Intrabasin faults are cemented principally by silica or carbonate minerals. Silica cements are limited to fault zones in the northwestern part of the Santo Domingo Basin mainly north of the Jemez River and west of the Rio Grande (fig. E12), where they become more concentrated northward towards the Jemez volcanic field. In the La Bajada constriction area silica cement is present along the northern San Francisco (SF), Sile (SI), and South Pajarito (SP) faults (fig. E12). Silica-cemented portions of fault zones commonly form prominent topographic ribs or ridges. Silica cements include microcrystalline cristobalite (or tridymite) and opaline and chalcedonic silica. On the basis of the mineralogy and spatial restriction of the silica cements, we infer that the cements precipitated from hydrothermal fluids flowing southward, downgradient, and possibly upwards along faults emanating from magmatic centers within the Jemez volcanic field.

Carbonate cements, mostly micritic and less common sparry calcite, are widely distributed in the Santo Domingo Basin (fig. E12) (see also Mozley and Goodwin, 1995; Heynekamp and others, 1999). Fault-zone sandstones that are strongly cemented with calcite commonly stand out in positive topographic relief. Concentrated calcite cements are also expressed as spherical to spherulitic concretions that weather into balls as much as several centimeters in diameter, but elongate carbonate cement concretions such as those used by Mozley and Goodwin (1995) to infer the orientation of ancient ground-water flow are rarely observed. Both carbonate and silica cements occupy some fault zones in the northern part of the study area, and contact and crosscutting relations indicate that the carbonate mostly precipitated later than the silica. The most strongly carbonate-cemented fault zones are located south of the area of silica cement in the southern Santo Domingo and northern Albuquerque Basins (fig. E12). In the La Bajada constriction area the Borrego (BR), Sile (SI), South Pajarito (SP), San Francisco (SF), and La Bajada (LB) fault zones are locally well cemented with carbonate (fig. E12).

Most fault zones are asymmetrically cemented; the cements are localized on one side of the fault in the mixed zone and in sand-rich portions of the adjacent fault core (fig. E12). Some cements extend into the inner part of the hanging-wall or footwall damage zone, but they rarely continue beyond the outer edge of the damage zone. The restriction of strongly cemented zones to one side of fault zones for considerable distance along strike (as much as 15 km) suggests that the faults localized or channeled the flow of fluids rather than fortuitously juxtaposing cemented and uncemented stratigraphic intervals. However, where protoliths have been cemented during diagenesis, fault-controlled cement is difficult to distinguish from previously existing cement in beds that were entrained in the fault zone.

In some parts of the basin, cement asymmetry locally alternates across a series of adjacent fault blocks. For example, opposing silica cement asymmetries are observed along the Sile (SI) and San Francisco (SF) faults in the La Bajada constriction area (fig. E12). The northern San Francisco fault and the aligned end of the oppositely dipping South Pajarito fault (SP) to the north are both silica cemented on their west sides, whereas the neighboring Sile fault is cemented on its east side (fig. E12). Such closely spaced reversals in cement asymmetry strongly suggest local fault-baffled or -compartmentalized ancient flow, and a regional hydrologic gradient was locally modified owing to fault permeability structures that acted as both conduits and barriers. The Sile (SI) and South Pajarito (SP) faults contain separate zones of silica and carbonate cement on opposite sides of their respective fault zones (fig. E12), suggesting that earlier cemented (silica?) zones acted as seals to later (carbonate-bearing?) ground-water flow.

Evidence of recurring fault cementation and fracturing is provided by numerous observations of one or more generations of cemented veins and fractures that cut earlier cemented sediments within the mixed zone, presumably owing to the effects of episodic fault deformation concentrated near the fault cores. Parts of fault zones that once focused fluid flow eventually became cemented and are now zones of lower permeability, unless the cements themselves developed opening-mode fractures during renewed fault movements. Strong cementation of fault zones that have not experienced refracturing has shifted the regions of highest relative permeability away from the cemented zones and low-permeability fault core, presumably laterally toward the outer damage zone, and in some cases to the other side of the fault zone.

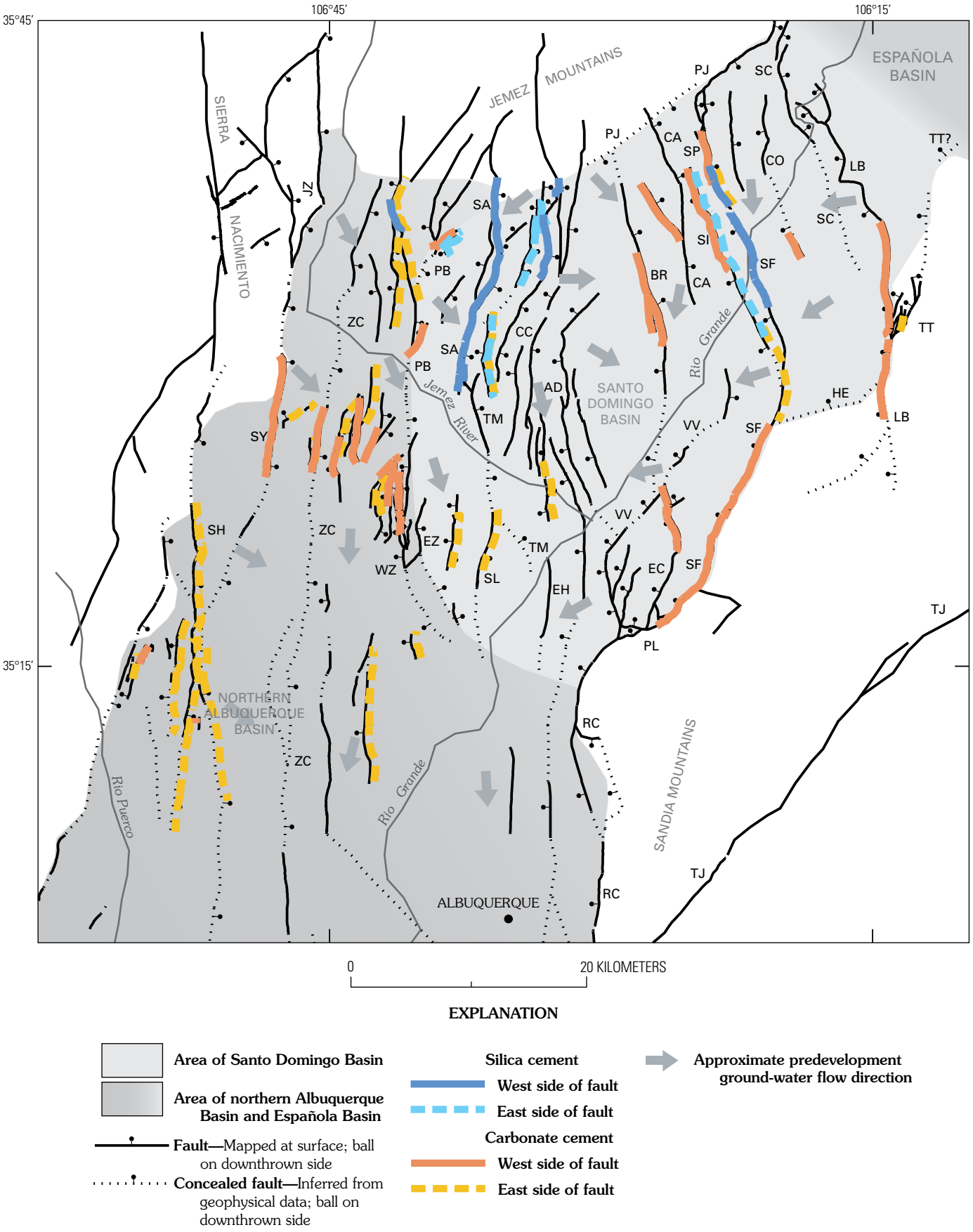
106°45′
106°15′
35°45′
35°15′
SIERRA NACIMIENTO
JEMEZ MOUNTAINS
ESPAÑOLA BASIN
SANTO DOMINGO BASIN
NORTHERN ALBUQUERQUE BASIN
SANDIA MOUNTAINS
Rio Grande
Jemez River
Rio Puerco
ALBUQUERQUE
JZ
SA
PB
ZC
CC
AD
TM
SY
SH
EZ
WZ
SL
EH
VV
EC
SF
PL
RC
PJ
CA
SP
CO
LB
SC
SI
BR
TT?
TT
HE
TJ
0
20 KILOMETERS
EXPLANATION
Area of Santo Domingo Basin
Area of northern Albuquerque Basin and Española Basin
Fault—Mapped at surface; ball on downthrown side
Concealed fault—Inferred from geophysical data; ball on downthrown side
Silica cement
West side of fault
East side of fault
Carbonate cement
West side of fault
East side of fault
Approximate predevelopment ground-water flow direction

Figure E12 (facing page). Santo Domingo Basin region showing asymmetrically distributed carbonate and silica fault zone cements. Silica cement is restricted to northern Santa Domingo Basin along faults near Jemez volcanic field, whereas carbonate cement is distributed throughout basin. Fault cement asymmetries show no systematic pattern relative to basin positions and modern ground-water flow directions (thick gray arrows). Flow directions based on water-elevation map of Bexfield and Anderholm (2000). Faults and fault zones: AD, Algodones; BR, Borrego; CA, Camada; CC, Cañada de Cochiti; CO, Cochiti; EC, Escala; EH, East Heights; EZ, East Ziana; HE, Hagan Embayment; JZ, Jemez; LB, La Bajada; PB, Pico Butte; PJ, Pajarito; PL, Placitas; RC, Rincon; SA, Santa Ana; SC, Sanchez; SH, Sand Hill; SI, Sile; SF, San Francisco; SL, South Luce; SP, South Pajarito; SY, San Ysidro; TJ, Tijeras; TM, Tamaya; TT, Tetilla; VV, Valley View; WZ, West Ziana; ZC, Zia County Dump.

Hydrogeologic Summary

Fault zones observed in the Santo Domingo Basin area are characterized by (1) outer damage zones that typically contain strike-parallel deformation bands and open extensional and shear fractures that may enhance or impede ground-water flow along the faults; (2) mixed zones composed of entrained and partly dismembered blocks of protolith rock or sediment; and (3) centrally positioned, low permeability, clay-rich fault cores that likely impede cross-fault flow. Protolith lithology strongly influences fault-zone architecture and component widths and controls variations in fracturing and other brittle-strain features.

Cements, recognized as a proxy for concentrated flow of ancient ground water, are common along fault zones in the basin. Silica cements are limited to faults that emanate from the Jemez volcanic field north of the basin, whereas carbonate fault cements are widely distributed. Coarse sediments (gravel and sand) host the greatest cement concentrations within fault zones; cements are also concentrated along open fractures and, to a lesser degree, along shear fractures and deformation bands within inner damage zones. Cements are commonly concentrated on one side of a fault and thus cement the fault zone asymmetrically. From observed spatial patterns of asymmetrically distributed fault zone cements, we infer that fault-parallel and -compartmentalized ground-water flow was, and may continue to be, common in the basin aquifers.

Our study indicates that the Santo Domingo Basin is densely populated with faults of various geometry, internal structure, and cement distribution. These aspects of the faults impart considerable heterogeneity of permeability within the basin aquifer. The types and statistical range of fault zone features appear to be consistent throughout the basin, a fact that is useful in creating simulations of ground-water flow that incorporate the influence of faults.

References Cited

Acocella, Valerio, Gudmundsson, Agust, and Funiciello, Renato, 2000, Interaction and linkage of extension fractures and normal faults—Examples from the rift zone of Iceland: Journal of Structural Geology, v. 22, p. 1233–1246.

Aldrich, M.J., Jr., 1986, Tectonics of the Jemez lineament in the Jemez Mountains and Rio Grande rift: Journal of Geophysical Research, v. 91, no. B2, p. 1753–1762.

Aldrich, M.J., Jr., Chapin, C.E., and Laughlin, A.W., 1986, Stress history and tectonic development of the Rio Grande rift, New Mexico: Journal of Geophysical Research, v. 91, no. B6, p. 6199–6211.

Baldridge, W.S., Ferguson J.F., Braile, L.W., Wang, Bin, Eckhardt, Kristine, Evans, David, Schultz, Craig, Gilpin, Bernard, Jiracek, G.R., and Biehler, Shawn, 1994, The western margin of the Rio Grande rift in northern New Mexico—An aborted boundary?: Geological Society of America Bulletin, v. 105, p. 1538–1551.

Bartolino, J.R., and Cole, J.C., 2002, Ground-water resources of the Middle Rio Grande Basin, New Mexico: U.S. Geological Survey Circular 1222, 132 p.

Besse, Jean, and Courtillot, Vincent, 1991, Revised and synthetic apparent polar wander paths for the African, Eurasian, North American and Indian plates, and true polar wander since 200 Ma: Journal of Geophysical Research, v. 96, p. 4029–4050.

Bexfield, L.M., and Anderholm, S.K., 2000, Predevelopment water-level map of the Santa Fe Group aquifer system in the middle Rio Grande Basin between Cochiti Lake and San Acacia, New Mexico: U.S. Geological Survey Water-Resources Investigations Report 00–4249, 1 sheet.

Buck, W.R., Lavier, L.L., and Poliakov, A.N., 1999, How to make a rift wide: Philosophical Transactions of the Royal Society [London], v. 357, p. 671–693.

Caine, J.S., Evans, J.P., and Forster, C.B., 1996, Fault zone architecture and permeability structure: Geology, v. 24, p. 1025–1028.

Caine, J.S., and Forster, C.B., 1999, Fault zone architecture and fluid flow—Insights from field data and numerical modeling, *in* Haneberg, W.C., Mozley, P.S., Moore, J.C., and Goodwin, L.B., eds., Faults and subsurface fluid flow in the shallow crust: American Geophysical Union Geophysical Monograph 113, p. 101–127.

Caine, J.S., Minor, S.A., Grauch, V.J.S., and Hudson, M.R., 2002, Potential for fault zone compartmentalization of groundwater aquifers in poorly lithified, Rio Grande rift-related sediments, New Mexico [abs.]: Geological Society of America Abstracts with Programs, v. 34, no. 4, p. 59.

Caine, J.S., Minor, S.A., and Hudson, M.R., 2004, On the lack of geochemical anomalies associated with faulting in poorly lithified, siliciclastic Santa Fe Group sediments, NM [abs.], *in* Hudson, M.R., ed., Geologic and Hydrogeologic Framework of the Española Basin—3d Annual Española Basin Workshop, Santa Fe, New Mexico, March 2–3, 2004, Proceedings: U.S. Geological Survey Open-File Report, OF–2004–1093, p. 26.

Cather, S.M., 1992, Suggested revisions to the Tertiary tectonic history of north-central New Mexico: New Mexico Geological Society 43d field conference, San Juan Basin IV, Guidebook, p. 109–122.

Cather, S.M., 1997, Constraints of Mesozoic piercing points on magnitude of northward Laramide translation of Colorado Plateau in north-central New Mexico: New Mexico Geology, v. 19, p. 50.

Chamberlin, R.M., 1999, Partitioning of dextral slip in an incipient transverse shear zone of Neogene age, northwestern Albuquerque Basin, Rio Grande rift, New Mexico [abs.]: Geological Society of America Abstracts with Programs, v. 31, no. 7, p. 113.

Chapin, C.E., and Cather, S.M., 1994, Tectonic setting of the axial basins of the northern and central Rio Grande rift, *in* Keller, G.R., and Cather, S.M., eds., Basins of the Rio Grande rift—Structure, stratigraphy, and tectonic setting: Geological Society of America Special Paper 291, p. 5–25.

Childs, Conrad, Watterson, Juan, and Walsh, J.J., 1995, Fault overlap zones within developing normal fault systems: Journal of the Geological Society [London], v. 152, p. 535–549.

Connell, S.D., Cather, S.M., Karlstrom, K.E., Read, A., Ilg, B., Menne, B., Picha, M.G., Andronicus, C., Bauer, P.W., and Anderson, O.J., 1995, Geology of the Placitas 7.5 minute quadrangle, Sandoval County, New Mexico: New Mexico Bureau of Mines and Mineral Resources Open-file Digital Map 2, scale 1:12,000.

Connell, S.D., Koning, D.J., and Cather, S.M., 1999, Revisions to the stratigraphic nomenclature of the Santa Fe Group, northwestern Albuquerque Basin, New Mexico: New Mexico Geological Society 50th field conference, Albuquerque Geology, Guidebook, p. 337–353.

Deamer, G.A., and Kodama, K.P., 1990, Compaction-induced inclination shallowing in synthetic and natural clay-rich sediments: Journal of Geophysical Research, v. 95, p. 4511–4529.

Demarest, H.H., 1983, Error analysis of the determination of tectonic rotation from paleomagnetic data: Journal of Geophysical Research, v. 88, p. 4321–4328.

Faulds, J.E., and Varga, R.J., 1998, The role of accommodation zones and transfer zones in the regional segmentation of extended terranes, *in* Faulds, J.E., and Stewart, J.H., eds., Accommodation zones and transfer zones—The regional segmentation of the Basin and Range Province: Geological Society of America Special Paper 323, p. 1–45.

Fisher, R.A., 1953, Dispersion on a sphere: Proceedings of the Royal Society [London], Series A217, v. 295–305.

Freund, Raphael, 1970, Rotation of strike-slip faults in Sistan, southeast Iran: Journal of Geology, v. 78, p. 188–200.

Gardner, J.N., and Goff, Fraser, 1984, Potassium-argon dates from the Jemez volcanic field— Implications for tectonic activity in the north-central Rio Grande rift: New Mexico Geological Society 35th field conference, Rio Grande Rift, Northern New Mexico, Guidebook, p. 75–81.

Grauch, V.J.S., 1999, Principal features of high-resolution aeromagnetic data collected near Albuquerque, New Mexico: New Mexico Geological Society 50th field conference, Albuquerque Geology, Guidebook, p. 115–118.

Grauch, V.J.S., Gillespie, C.L., and Keller, G.R., 1999, Discussion of new gravity maps for the Albuquerque Basin area: New Mexico Geological Society 50th field conference, Albuquerque Geology, Guidebook, p. 119–124, plates C and D, p. 136–137.

Grauch, V.J.S., Hudson, M.R., and Minor, S.A., 2001, Aeromagnetic expression of faults that offset basin fill, Albuquerque Basin, New Mexico: Geophysics, v. 66, no. 3, p. 707–720.

Hamilton, W.B., and Myers, W.B., 1966, Cenozoic tectonics of the western United States: Reviews of Geophysics, v. 4, p. 509–549.

Heynekamp, M.R., Goodwin, L.B., Mozley, P.S., and Haneberg, W.C., 1999, Controls on fault-zone architecture in poorly lithified sediments, Rio Grande rift, New Mexico—Implications for fault-zone permeability and fluid flow, *in* Haneberg, W.C., Mozley, P.S., Moore, J.C., and Goodwin, L.B., eds., Faults and subsurface fluid flow in the shallow crust: American Geophysical Union Geophysical Monograph 113, p. 27–49.

Housen, B.A., and van der Pluijm, B.A., 1991, Slaty cleavage development and magnetic anisotropy fabrics: Journal of Geophysical Research, v. 96, p. 9937–9946.

Hrouda, František, 1982, Magnetic anisotropy of rocks and its application in geology and geophysics: Geophysical Surveys, v. 5, p. 37–82.

Hudson, M.R., Minor, S.A., Grauch, V.J.S., and Personius, S.F., 1999, Preliminary characterization of faults in the middle Rio Grande Basin [abs.], *in* Bartolino, J.R., ed., U.S. Geological Survey Middle Rio Grande Basin Study: U.S. Geological Survey Open-File Report 99–203, p. 40–41.

Karlstrom, K.E., Cather, S.M., Kelley, S.A., Heizler, M.T., Pazzaglia, F.J., and Roy, M., 1999, Sandia Mountains and

Rio Grande rift—Ancestry of structures and history of deformation: New Mexico Geological Society 50th field conference, Albuquerque Geology, Guidebook, p. 155–165.

Kelley, V.C., 1977, Geology of Albuquerque Basin, New Mexico: New Mexico Bureau of Mines and Mineral Resources Memoir 33, 60 p.

Kelley, V.C., 1982, The right-relayed Rio Grande rift, Taos to Hatch, New Mexico: New Mexico Geological Society 33d field conference, Albuquerque Country II, Guidebook, p. 147–151.

Knipe, R.J., 1993, The influence of fault zone processes and diagenesis on fluid flow, *in* Horbury, A.D., and Robinson, A.G., eds., Diagenesis and basin development: American Association of Petroleum Geologists Studies in Geology 36, p. 135–148.

May, S.J., and Russell, L.R., 1994, Thickness of the syn-rift Santa Fe Group in the Albuquerque Basin and its relation to structural style, *in* Keller, G.R., and Cather, S.M., eds., Basins of the Rio Grande rift—Structure, stratigraphy, and tectonic setting: Geological Society of America Special Paper 291, p. 113–124.

Minor, S.A., and Hudson, M.R., 2006, Regional survey of structural properties and cementation patterns of fault zones in the northern part of the Albuquerque Basin, New Mexico: Implications for ground-water flow: U.S. Geological Survey Professional Paper 1719, 28 p.

Minor, S.A., and Sawyer, D.A., 1999, Structural evolution of a rift border fault zone—La Bajada fault zone, Rio Grande rift, northern New Mexico [abs.]: Geological Society of America Abstracts with Programs, v. 31, no. 7, p. 112.

Mozley, P.S., and Goodwin, L.B., 1995, Patterns of cementation along a Cenozoic normal fault—A record of paleoflow orientations: Geology, v. 23, p. 539–542.

Olson, J.E., and Pollard, D.D., 1989, Inferring paleostresses from natural fracture patterns—A new method: Geology, v. 17, p. 345–348.

Rawling, G.C., Goodwin, L.B., and Wilson, J.L., 2001, Internal architecture, permeability structure, and hydrologic significance of contrasting fault-zone types: Geological Society of America Bulletin, v. 29, no. 1, p. 43–46.

Russell, L.R., and Snelson, S., 1994, Structure and tectonics of the Albuquerque Basin segment of the Rio Grande rift—Insights from reflection seismic data, *in* Keller, G.R., and Cather, S.M., eds., Basins of the Rio Grande rift—Structure, stratigraphy, and tectonic setting: Geological Society of America Special Paper 291, p. 83–112.

Sawyer, D.A., Shroba, R.R., Minor, S.A., and Thompson, R.A., 2002, Geologic map of the Tetilla Peak 7.5 minute quadrangle, Santa Fe and Sandoval Counties, New Mexico: U.S. Geological Survey Miscellaneous Field Studies Map MF–2352, scale 1:24,000.

Sibson, R.H., 1996, Structural permeability of fluid-driven fault-fracture meshes: Journal of Structural Geology, v. 18, p. 1031–1042.

Smith, G.A., and Kuhle, A.J., 1998, Hydrostratigraphic implications of new geologic mapping in the Santo Domingo Basin, New Mexico: New Mexico Geology, v. 20, p. 21–27.

Smith, G.A., McIntosh, William, and Kuhle, A.J., 2001, Sedimentologic and geomorphic evidence for seesaw subsidence of the Santo Domingo accommodation-zone basin, Rio Grande rift, New Mexico: Geological Society of America Bulletin, v. 113, p. 561–574.

Wawrzyniec, T.F., Geissman, J.W., Melker, M.D., and Hubbard, Mary, 2002, Dextral shear along the eastern margin of the Colorado Plateau—A kinematic link between Laramide contraction and Rio Grande rifting (ca. 75–13 Ma): Journal of Geology, v. 110, p. 305–324.

Wernicke, Brian, 1992, Cenozoic extensional tectonics of the U.S. Cordillera, *in* Burchfiel, B.C., Lipman, P.W., and Zoback, M.L., eds., The Cordilleran orogen—Conterminous U.S.: Geological Society of America, The geology of North America, v. G-3, p. 553–581.

Woodward, L.A., 1977, Rate of crustal extension across the Rio Grande rift near Albuquerque, New Mexico: Geology, v. 5, p. 269–272.

Zoback, M.L., Anderson, R.E., and Thompson, G.A., 1981, Cainozoic evolution of the state of stress and style of tectonism of the Basin and Range Province of the western United States: Philosophical Transactions of the Royal Society [London], v. 300, p. 407–434.

Published in the Central Region, Denver, Colo.
Manuscript approved for publication February 10, 2006
Graphics by authors
Photocomposition by Mari L. Kauffmann (Contractor, ATA Services)
Edited by Mary-Margaret Coates (Contractor, ATA Services)